

Gas phase synthesis of isopropyl chloride from isopropanol and HCl over alumina and flexible 3-D carbon foam supported catalysts

Natalia Bukhanko, Christopher Schwarz, Ajaikumar Samikannu, Tung Ngoc Pham, William Siljebo, Johan Wärnå, Andrey Shchukarev, Anne-Riikka Rautio, Krisztian Kordás, Jyri-Pekka Mikkolaa,

Isopropyl chloride synthesis from isopropanol and HCl in gas phase over ZnCl₂ catalysts supported on Al₂O₃ as well as flexible carbon foam was studied in a continuous reactor. A series of catalytic materials were synthesised and characterised by BET, XPS, SEM, TEM, XRD and NH₃-TPD methods. Catalytic activity tests (product selectivity and conversion of reactants) were performed for all materials and optimal reaction conditions (temperature and feedstock flow rates) were found. The results indicate that the highest yield of isopropyl chloride was obtained over 5 wt.% ZnCl₂ on commercial Al₂O₃ (No. II) (95.3%). Determination of product mixture compositions and by-product identification were done using a GC-MS method. Carbon foam variant catalyst, 5 wt.% ZnCl₂/C, was found to perform best out of the carbon-supported materials, achieving ~75% yield of isopropyl chloride. The kinetic model describing the process in a continuous packed bed reactor was proposed and kinetic parameters were calculated. The activation energy for the formation of isopropyl chloride reaction directly from isopropanol and HCl was found to be ~58 kJ/mol.

Nomenclature

C	concentration
D_i	diffusion coefficient
E_a	activation energy
K	rate constant
K_{eq}	equilibrium constant
L	radius of pellet
m_{cat}	catalyst mass
n_i	molar flow of i -th component
r_i	component generation rates
R	gas constant
T	temperature
w_{cat}	catalyst weight fraction
η	effectiveness factor
ϕ	Thiele modulus
ρ_B	catalyst bulk density

List of symbols

i -PrCl isopropyl chloride

i-PrOH isopropanol

List of indexes

Cat catalyst

I component index

1. Introduction

Short-chain chloroalkanes are known as compounds that play an important role in modern chemical industry. Among other uses, they are used as refrigerants, local anaesthetics (ethyl chloride [1,2] and isopropyl chloride [3,4]) and as reactants in alkylation, synthesis of ionic liquids and cellulose derivatives [2,5,6]. Two main routes are widely used upon isopropyl chloride production – hydrochlorination of propylene over different catalysts (such as alumina, FeCl₃, hydrochlorinated alumina, tellurium compounds) and hydrochlorination of isopropanol over zinc chloride or aluminosilicate catalysts [7–16]. Hydrochlorination of alkenes and primary alcohols to synthesise corresponding primary alkyl halides is more preferable than chlorination because of environmental reasons [17–23]. Esterification of primary alcohols (methanol, ethanol) over highly porous and non-toxic alumina catalysts was found to be the most environmentally friendly, modern, and efficient route [20–23]. This method can also be considered as “green” when utilising bio-alcohols (produced by biomass fermentation) as feedstock [24–27]. Tundo et al. reported about hydrochlorination of primary alcohols with longer chains (n-propanol, nbutanol and n-pentanol) over Lewis acid catalysts supported by silica gel [28]. The reaction kinetics of primary alkyl chlorides synthesis processes was studied only for methyl and ethyl chlorides [18–23]. The reaction of isopropanol hydrochlorination has earlier only been studied in liquid phase over ZnCl₂ catalysts, resulting in relatively low conversion of reactants to products, low product selectivity and facilitating the need of a separation process [11,12,29]. The reaction kinetics and mechanism were studied for the reaction of isopropanol with HCl in liquid phase only [29]. Thus, the limited information about the process of gas-phase isopropyl chloride synthesis renders it more interesting to investigate. Application of highly porous alumina supported catalysts for hydrochlorination of alcohols is as a versatile, advanced and environmentally safe way to reach the highest conversion and selectivity towards chloride.

Besides alumina, powdered or pelletised activated carbon has also been used as catalyst support for hydrochlorination reactions in a few studies [30–33]. In our study, for the first time, monolithic carbon foam was used as a catalyst support in the hydrochlorination reaction of isopropanol. Created from melamine foam, the flexible, 3D-structured carbon foam possesses a lot of interesting properties such as low density, high compressibility and high surface area. Moreover, polar groups such as carboxyl and hydroxyl groups on its surface can be utilised to immobilise metal nanoparticles on the surface. The aforementioned characteristics allow the carbon foam to be adapted to various purposes, especially as catalyst support in gas and liquid phase reactions [34,35]. In this work, ZnCl₂ was decorated onto the surface of monolithic carbon foam by the incipient wetness impregnation method and the prepared catalyst was then used in the isopropanol hydrochlorination to isopropyl chloride.

The gas-phase synthesis of isopropyl chloride from isopropanol and HCl was performed in a packed bed reactor over *x* wt.% ZnCl₂/Al₂O₃ (*x*=0, 2, 5) and *y* wt.% ZnCl₂/C (*y*=2, 5, 10) catalysts. Three types of alumina support, tailor-made highly porous alumina and two commercial alumina supports with different particle size distribution were utilised. In addition, a carbon sponge impregnated with ZnCl₂ was tried as an alternative catalyst formulation. The main goal of this work was to examine the feasibility of the process

and to find the optimal process conditions, resulting in highest reactants conversion and product selectivity. The kinetic model for the isopropanol hydrochlorination reaction in a packed-bed reactor is presented and a reaction mechanism in comparison with those for other primary alcohols is proposed.

2. Experimental

2.1. Catalysts preparation

To perform the reaction of isopropanol hydrochlorination, four types of catalytic support were used. Highly porous aluminium oxide prepared by a sol–gel method [20] was used as the catalyst support for the materials of first group. The commercial Al_2O_3 , fraction $z < 250 \mu\text{m}$ and fraction $250 < z < 500 \mu\text{m}$ named as No. I and No. II, respectively, were used as supports for the materials of second group. Melamine derived carbon sponge was used as a support for materials of third group [34]. Zinc chloride salt (analytical grade, >98%, Merck) was used for the preparation of the modified catalysts. The reactants were isopropyl alcohol (99.8% analytical grade) and gaseous HCl anhydrous (99.999%, PRAXAIR).

The highly porous Al_2O_3 was prepared via a solvothermal technique, the synthesis details of which can be found in our previous work [20]. The modified alumina catalysts $x \text{ wt.}\% \text{ ZnCl}_2 / \text{Al}_2\text{O}_3$ ($x=0, 2, \text{ and } 5$) were prepared by means of the impregnation method for highly porous Al_2O_3 support and both of commercial Al_2O_3 supports No. I and No. II.

Monolithic carbon foam supported materials were prepared by the technique described by Pham et al. [34]. In short, the melamine-based polymer foam (BASF, Basotect® G, used as received) was pyrolysed at $800 \text{ }^\circ\text{C}$ during 1 h with a ramping rate of $1 \text{ }^\circ\text{C}/\text{min}$ in a tubular quartz reactor under nitrogen flow ($50 \text{ mL}/\text{min}$). Then the material underwent an activation process at $800 \text{ }^\circ\text{C}$ with CO_2 ($1 \text{ mL}/\text{min}$, 2 vol.% in N_2) for 2 h. As the next step, the system was cooled down to room temperature in an inert atmosphere (N_2).

The $y \text{ wt.}\% \text{ ZnCl}_2/\text{C}$ ($y= 2, 5 \text{ and } 10$) catalysts were prepared by the incipient wetness impregnation method. Generally, a calculated amount of ZnCl_2 was dissolved in 35 mL of Milli-Q water and 0.25 g carbon foam was then dipped into the solution for 4 h. Finally, wet catalyst was oven dried overnight at $100 \text{ }^\circ\text{C}$ in air.

2.2. Catalysts characterisation

To characterise catalytic materials before and after use in the reaction, various surface characterisation techniques like X-ray photoelectron spectroscopy (XPS), transmission electron microscopy (TEM), scanning electron microscopy (SEM), X-ray diffraction (XRD), nitrogen physisorption and ammonia temperature programmed desorption ($\text{NH}_3\text{-TPD}$) techniques were employed.

The morphology of catalytic materials before and after their test in the reactions was examined by LEO 912 OMEGA energy filtered TEM operating at 120 kV.

Scanning electron microscopy (SEM) measurements were carried out using a Zeiss Merlin FEG-SEM instrument operating at 4 kV.

Surface composition of catalytic materials before and after reaction was studied by the XPS technique. All XPS spectra were recorded with a Kratos Axis Ultra electron spectrometer equipped with a delay line detector. A monochromatic $\text{AlK}\alpha$ source operated at 150 W, hybrid lens system with magnetic lens, proving an analysis area of $0.3 \text{ mm} \times 0.7 \text{ mm}$, and charge neutraliser were used for the measurements. The binding energy scale was referenced to the C 1s line of aliphatic carbon, set at 285.0 eV. Processing of the spectra was accomplished with the Kratos software.

Phase composition of catalytic materials was analysed by powder XRD (Siemens D5000 XRD, CuK α radiation). The recording was carried in the range 2 θ angles from 5° to 80° at a scanning speed of 0.5°/min. Identification of phase composition was performed using Diffract-plus EVA database (Bruker).

The pore diameter, pore volume and surface area of the carbon supports and the catalyst materials were measured at 77 K in a Micromeritics Tristar 3000 Surface Area and Porosity analyser by N₂ adsorption – desorption method (nitrogen physisorption). For alumina based catalyst, around 0.2 – 0.5 g sample was degassed in nitrogen flow at 200 °C for 2 h to remove the moisture from the pores of the material. In the case of carbon-based catalysts, two degassing conditions were used: normal (120 °C for 2 h in nitrogen flow) and intensive (200 °C for 4 h in nitrogen flow). The pore diameter and pore volume were calculated from the adsorption isotherms using the BJH method. The surface area was calculated using the adsorption data up to a relative pressure of 0.2 by the Brunauer-Emmett-Teller (B.E.T.) method.

Number of acid sites on alumina-based catalysts was determined by the temperature-programmed desorption of ammonia (NH₃-TPD) method using Micromeritics AutoChem 2910 analyser. Degassing was performed at 120 °C in a helium flow during 120 min; then the system was cooled down up to 100 °C. Ammoniation procedure was performed by absorbing of mixture consisted of 5% NH₃ and 95% He at 100 °C during 60 min. The excess of ammonia was flushed out for 60 min at 100 °C. The system was heated at heating rate of 10 °C/min up to 900 °C and TCD were recorded. The acidity was calculated as a ratio of peak areas of sample to peak area of ammonia absorbed multiplied with number of moles of ammonia used for calibration.

2.3. Catalytic experiments

The corrosion-resistant fixed-bed reactor (ID 10 mm, length 260 mm) constructed from a stainless steel tube with tantalum lining inside was used to perform catalytic experiments. The catalyst was heated overnight at the reaction temperature under nitrogen flow to remove moisture from the reactor system. The reactor temperature was controlled by external heaters along the reactor system. Two thermocouples were placed inside the reactor, well extending to the catalyst bed ($m_{cat} = 0.25$ g, $l_{bed} = 3$ cm) and used to monitor the reaction temperature. Glass beads were applied as spacers in the reactor. Isopropyl alcohol was fed with an HPLC-pump and vaporised at 150 °C before entering the reactor. Different reaction temperatures (150, 170, 180 and 200 °C) were tested but only 170 and 180 °C were found to be optimal temperature conditions. All experiments were performed under atmospheric pressure. The molar ratio of feedstock used was $n_{i-PrOH}:n_{HCl} = 1:1$ and $1.05:1$. The gaseous HCl flow rate was controlled by means of a mass-flow controller and was calibrated before each experiment. The flow of HCl was turned on first to pre-treat and activate catalyst surface and after 2–3 min isopropanol flow was turned on. The mixture of products from the reactor outlet was passed through a desiccant (CaO powder mixed with Raschig rings for higher contact area heated to 100–105 °C) to remove unreacted HCl. The reaction products were collected in a cold trap ($T = -5$ to 0 °C) and the samples for analysis were withdrawn every 15 min with a cooled syringe (0 °C) because of the high volatility of isopropyl chloride ($T_{b.p.} = 34–36$ °C). The condensed liquid-phase products were analysed by means of Gas Chromatography (GC, Agilent 6890N). The device was equipped with a flame ionisation detector (FID) and HP-PLOT/U capillary column (oven temperature 180 °C, isothermal). Identification of unknown components was performed by GC-MS analysis (Agilent Technologies GC model No. 7820A coupled to MSD model No. 5975) using the same HP-PLOT/ U capillary column. All samples were mixed with methanol before analysis.

The yield of *i*-PrCl (Y_{i-PrCl}) was estimated as the ratio of the FID peak area of isopropyl chloride to the total area of all sample compounds (isopropanol, isopropyl chloride, diisopropyl ether, propylene and minor by-products).

The product selectivity Si-PrCl was calculated as the ratio of the FID peak area of the isopropyl chloride to the total area of all products (isopropyl chloride, diisopropyl ether, propylene and minor products).

Before GC analysis of products mixture and calculation of yield and conversion values FID detector was calibrated by means of calculation of response factor C for i-PrCl/i-PrOH and diisopropyl ether/i-PrOH pairs to be able to use the values of chromatograms peak areas for estimation of the yield and selectivity values. The calibration was performed by GC analysis of standard mixtures, contained known concentrations of target components – isopropyl chloride/isopropanol and diisopropyl ether/isopropanol. The response factors were calculated as ratios:

$$C_1 = \frac{A_{i-PrCl} \cdot \chi_{i-PrOH}}{A_{i-PrOH} \cdot \chi_{i-PrCl}}$$

$$C_2 = \frac{A_{diisopropyl\ ether} \cdot \chi_{i-PrOH}}{A_{i-PrOH} \cdot \chi_{diisopropyl\ ether}}$$

where A is peak areas, x is molar % of the component in standard mixture and consisted $C_1 = 0.696$ for i-PrCl/i-PrOH and $C_2 = 0.432$ for diisopropyl ether/i-PrOH, respectively.

2.4. Acid–base titration procedure

To verify the conversion rates obtained from GC data (based on a carbon mass balance), the reactor output was periodically monitored using an automated titration system (developed at Umeå University as a student project) to measure the outflow of unreacted HCl. The titration system consisted of a neutralisation vessel with stirrer, a peristaltic dosing pump for NaOH solution, and a pH electrode connected to a pHstat set to maintain pH 6. The HCl conversion X_{HCl} (%) was calculated using the formula:

$$X_{HCl} = \left(1 - \frac{\dot{n}(HCl)_{out}}{\dot{n}(HCl)_{in}}\right) \cdot 100\%.$$

The flow $\dot{n}(HCl)_{out}$ was calculated as:

$$\dot{n}(HCl)_{out} = \frac{V_{NaOH} \cdot C_{NaOH}}{t},$$

2.5. GC-MS analysis

To identify all reaction products, GC-MS analysis was used. The measurements were performed under similar GC parameter settings and column type as prior GC-FID analysis in order to obtain same retention times ($T_{inlet} = T_{oven} = 180$ °C, flow rate 1 mL/min, injection volume 0,6 µL). Helium was used as carrier gas. The MS was operated with a source temperature of 250 °C, quadrupole scanning was performed over a range of 15–800 a.m.u. All accessories were cooled down to –5 °C to avoid the evaporation of volatile components, including isopropyl chloride. The analysis was performed on a sample produced over 5 wt. % ZnCl₂/Al₂O₃ (No. II) catalyst at T =180 °C, ni-PrOH:nHCl = 1:1, t =11825 min conditions after 120 h of reaction. Data were collected using MSD Chem station, E.02.02.1431 software package. NIST Library (version 2.0 g) was used for components identification.

3. Results and discussion

3.1. Structure and chemical composition of catalyst materials

For characterisation of catalytic materials before and after their using in the reaction, BET, XPS, XRD, TEM and NH₃-TPD analysis were used. The results are given in Tables 1–4 and are depicted in Figs. 1 and 2 and Figures 1–19 of Supplementary content.

The surface area, pore size and pore volume of the materials were measured by nitrogen physisorption method (B.E.T.). The results are given in Table 1 and in Figures 1–5 of Supplementary content. It is seen, that materials supported by high-porous Al₂O₃ (both pure and ZnCl₂-decorated) exhibited the highest surface area as expected, compared to both of commercial alumina supports. As a trend, spent materials exhibited substantially decreased surface area (around 30% both for 2 wt.% and 5 wt.% ZnCl₂-decorated) and pore size distribution whereas the pore volume increased. The surface area of 5 wt.% ZnCl₂/Al₂O₃ (No. II) catalyst was strongly decreasing (by up to 45%) upon long-time testing (11825 min) under reaction conditions. In case of experiments with higher product yield values (> 90%) apparently correlated with a slightly stronger decrease in catalyst surface area. Thus, in case of 5 wt. % ZnCl₂/Al₂O₃ catalyst (No. I), around 27% and in case of 5 wt.% ZnCl₂/Al₂O₃ (No. II) around 31% loss of pore surface area was typically recorded. Upon lower yield levels (< 82%), over the 5 wt.% ZnCl₂/Al₂O₃ catalyst (No. II), about 22% and in case of the catalyst 5 wt.% ZnCl₂/Al₂O₃ (high porous), about 17% of the surface area was lost during prolonged times-on-stream.

Figure 5 (Supplementary content) illustrates the results of B.E.T. analysis for carbon-based catalysts. The surface area of fresh catalyst was decreased from 322 m²/g to only 4.0 m²/g when increase ZnCl₂ loading from 2 to 10 wt.%. It is obvious that at 10 wt.% metal loading was beyond the loading capacity of the carbon foam. The pore blockage due to high metal loading also can be seen through the decreasing of pore volume, dropped from 1.2 to 0.06 cm³/g for 2 and 10 wt.% ZnCl₂ loading, respectively. It can be seen that a dramatic loss of the surface area upon reaction occurs, amounting to 97%. This effect might be happened due to blockage of the pores by water and also maybe by other chemicals strongly trapped inside small pores of the foam.

To get more information about the surface composition both fresh and spent catalytic materials were analysed by means of XPS. The results in case of 2 and 5 wt.% ZnCl₂/Al₂O₃ (all support types) and pure high porous alumina catalysts were compared and are shown in Table 2 as atomic ratios.

In case of all the catalysts, the trend was similar. Thus, the atomic ratio of Al–OH/Al–O does not changes upon the reaction for materials, containing 5 wt.% ZnCl₂ and slightly changed for materials, containing 2 wt.% of ZnCl₂. On the other hand, the Cl/Zn ratios as well as the Cl/Al were significantly increased upon exposure to the reaction conditions (except 2 wt.% ZnCl₂/Al₂O₃ (No. I), row 3, Table 3) whereas the Al/Zn ratio indicated the leaching of Zn. Indeed, the hypothesis that Zn plays an important but not the only role and influences the reaction mechanism is well agreeing with the literature.

The XPS atomic ratios for fresh and spent 5 wt.% ZnCl₂/C catalyst are given in Table 3. Both of atomic ratios, Cl/Zn and (C + N)/Zn abruptly increase after exposure to the reaction conditions. On the basis of these results, we can draw apparent conclusions about a crucial role of ZnCl₂ in terms of the reaction mechanism.

Phase composition of all catalyst materials both before and after reactions was characterised by XRD analysis. The diffractograms for alumina- and carbon supported materials are summarised and depicted in Figures 6–10 (Supplementary content). The relative intensities of the reflections from the crystallographic

planes of the identified phases such as $\text{AlO}(\text{OH})$, $\text{Al}_{10}\text{O}_{15}\cdot\text{H}_2\text{O}$ and $\gamma\text{-Al}_2\text{O}_3$ are marked with black, red and blue colours according to the most intensive peaks in the Reference cards 00-021-1307, 00-022-1119 and 00-050-0741, respectively.

It is seen that pure Al_2O_3 high porous catalysts are amorphous regardless whether they were analysed before or after use in the reaction. The fresh catalyst, 2 wt.% ZnCl_2 decorated Al_2O_3 high porous and its spent at 150 °C counterpart (blue line) are also amorphous. However, the other three spent materials, supported by commercial alumina No. I and No. II show some crystallinity with patterns matching mainly with aluminium oxide hydroxide ($\text{AlO}(\text{OH})$, 00-021-1307 card) and aluminium oxide hydrate ($\text{Al}_{10}\text{O}_{15}\cdot\text{H}_2\text{O}$, 00-022-1119 card) phases. Some weak ordering in the stoichiometric fcc γ -alumina phase ($\gamma\text{-Al}_2\text{O}_3$, 00-050-0741 card) is also suggested by the very diffuse scattering from the (4 0 0) crystal planes (Figure 6, Supplementary content).

Figures 7–10 (Supplementary content) depict the XRD data for all catalytic materials decorated by 5 wt.% of ZnCl_2 . The results are shown both for fresh and spent materials. It is seen that for impregnated commercial alumina materials 5 wt.% $\text{ZnCl}_2/\text{Al}_2\text{O}_3$ (No. I) and 5 wt.% $\text{ZnCl}_2/\text{Al}_2\text{O}_3$ (No. II), similar trends were observed: an increasing crystallinity of catalyst materials upon exposure to the reaction conditions. Thus, $\text{AlO}(\text{OH})$ and $\gamma\text{-Al}_2\text{O}_3$ phases were found in both of the samples. For the materials based on high porous alumina, only few ordered bcc aluminium oxyhydroxide ($\text{AlO}(\text{OH})$) species were observed. The presence of this phase was found both after short- and long-time testing of the catalyst under various reaction conditions. Moreover, no ZnCl_2 and/or ZnO_x phases were identified in this group of materials.

Compared to all other catalysts, in the fresh 5 wt.% $\text{ZnCl}_2/\text{Al}_2\text{O}_3$ highly porous catalyst fcc $\gamma\text{-Al}_2\text{O}_3$ phase was found in fresh material. No phases were detected in this material after its exposure to the reaction conditions and instead, the materials become amorphous. This was the main difference observed between the highly porous Al_2O_3 and both of commercial alumina materials.

The results of carbon-based materials (for the 5 wt.% ZnCl_2/C) are shown in Figure 10 (Supplementary content). As it can be seen, the catalyst material remained amorphous (both fresh and spent materials). However, three weak signals of unidentified phases appear after exposure to the reaction conditions. No ZnCl_2 signals could be identified for either of the materials.

Transmission electron microscopy was used to examine the surface morphology of fresh and spent 5 wt.% $\text{ZnCl}_2/\text{Al}_2\text{O}_3$ catalysts for all

three types of catalyst supports (Fig. 1a–g). For both of commercial Al_2O_3 (No. I) and (No. II) materials no large clusters were seen for indicating that the materials are homogeneous (Fig. 1a–e). The black arrows are pointing to (possible) nanoparticles, however it is extremely difficult to distinguish the ZnCl_2 particles from the amorphous alumina support as well as XRD data do not reveal any presence of zinc chloride and/or oxychlorides in the samples. Thus it may be concluded that the small nanoparticles of ZnCl_2 are homogeneously dispersed in alumina.

Compare TEM images of fresh and spent materials we can conclude that catalysts surface was not essentially altered during their using in the reaction. However, the distribution of ZnCl_2 particles (black arrows) on the surface is slightly changed for Al_2O_3 (No. I) and high porous alumina supports. It was also observed that the zinc chloride particle size on high porous alumina catalyst before and after reaction was smaller than for those on commercial Al_2O_3 (No. I) and (No. II) catalysts (Fig. 1f and g). For both of commercial catalysts the surface looks very similar before and after reaction (Fig. 1a–e). Commercial

support Al₂O₃ (No. II) looks different from high porous and (No. I) support due to changes with particle size after the reaction; however, no significant differences could be observed in the surface images after short-time and long-time reaction tests (Fig. 1d and e). For spent 5 wt.% ZnCl₂/Al₂O₃ (high porous) catalyst large particles were seen (black arrow in Fig. 1g). However, XRD could not detect the presence of ZnCl₂ or other zinc compounds so we can conclude that the ZnCl₂ is amorphous but not crystalline.

Ammonia adsorption/desorption is a process which allows to calculate total number of acid sites on catalyst surface without their identification as Brønsted or Lewis acid sites [36–39]. The total acidity values of the catalysts were determined from peak area correspond to one or several temperatures. Table 4, Fig. 2 and Figures 11–19 of Supplementary content summarise results of total acidity of all alumina-based catalysts, determined from ammonia temperature-programmed desorption peaks at different temperatures, which correspond to weak, medium and strong acids sites (Fig. 2). However, strong acids sites were not detected on TPD-profiles for all materials of highly porous alumina group whereas materials supported commercial aluminas (No. I) and (No. II) contained two (medium and strong) or three (weak, medium and strong) types of inhomogeneously distributed acid sites. The calculated values of total acidity (i.e. ammonia adsorbed/ desorbed amount) are in the range 20–28 mmol/g for all types of alumina supports.

3.2. Influence of reaction parameters and support type in terms of conversion and product selectivity

Two feedstock molar ratios n-i-PrOH:n-HCl were employed for the catalytic process of isopropanol hydrochlorination: equimolar (1:1) and with slight excess of isopropanol (1.05:1). The evaporated gaseous reactant mixture was passed through a fixed catalyst bed. At start up, the HCl gas flow was turned on and passed through the system in order to activate the catalyst surface [20,40] and consequently to increase the yield. After 2–3 min isopropanol flow was switched on. The temperatures were selected as 150, 170, 180 and 200 °C and was not raised further since there is no isopropyl chloride and other liquid by-products formed at elevated temperatures.

The results are tabulated in Table 5 for 30 experiments. For pure alumina catalysts the yield of i-PrCl was quite low; for commercial Al₂O₃ (No. I) catalyst the highest catalytic performance was a yield value of ~78% reached at 180 °C and low HCl flow rate 10 mL/min (Table 5, row 12). At a higher HCl flow rate of 20 mL/min the same material showed an essentially lower capacity and yield was about 25% (Table 5, row 11). Interesting is that another commercial Al₂O₃ (No. II) exhibited the same performance for all experimental conditions, yield reaching around 60% (Table 5, rows 18 and 19). Slightly higher difference was observed for highly porous alumina catalyst at 180 °C both at high and low HCl flow rates (71% and 61%, respectively, Table 5, rows 1 and 2). A slight decrease of i-PrCl yield down to 62.5% at low reaction temperature 170 °C was also observed (Table 5, row 3). The increase of reaction temperature to 200 °C led to a significant decrease in i-PrCl yield down to ~41% (Table 5, row 4) due to dominating formation of gaseous by-products. A significant difference of catalytic performance for highly porous and commercial alumina materials can be explained by the presence in last of γ -Al₂O₃ phase [20], with large number of Lewis acid sites which play a dominant role in isopropanol dehydration process [41,42].

Another situation was observed for the 2 wt.% ZnCl₂/Al₂O₃ catalysts. In this group, the best catalytic performance was reached over 2 wt.% ZnCl₂/Al₂O₃ (No. II) catalyst, where the yield was more than 80% both at 20 and 10 mL/min HCl flow rates (rows 21 and 22, Table 5). For highly porous alumina-based catalyst, the yield observed was very low at all the temperatures tested and did not exceed 60% (rows 5, 6, 7 and 8 in Table 5). The experiments over 2 wt.% ZnCl₂/Al₂O₃ (No. I) material show low yield values as

well (maximum around 70%, rows 13, 14 and 15 in Table 5). Thus we can conclude that the role of catalyst support type is essential when very low ZnCl_2 loadings are used.

It should be noted that the true selectivity and yield values might be overestimated because of potential loss of formed gaseous by-product, propylene. Due to differences in FID response factors of the analysed compounds, directly using peak areas from the chromatograms will also add a varying degree of overestimation to the calculated results. Estimated values will, however, converge with true values when approaching 100%.

In all the cases of alumina catalysts impregnated by 5 wt.% ZnCl_2 (No. I, No. II and highly porous), a significant increase in yield of i-PrCl can be seen, compared to the pure alumina supports and 2 wt.% $\text{ZnCl}_2/\text{Al}_2\text{O}_3$ materials. The yield value was increased from 71% in case of pure Al_2O_3 to ~90% in case of 5 wt.% $\text{ZnCl}_2/\text{Al}_2\text{O}_3$, at 180 °C, HCl flow rate 20 mL/min and equimolar reactant feed (rows 1 and 9, respectively, Table 5). However, in case of the 2 wt.% $\text{ZnCl}_2/\text{Al}_2\text{O}_3$ catalyst, we observed the lower yield to 48 % (row 7, Table 5) as over pure alumina at the same conditions.

The highest values of i-PrCl yield and process selectivity, ~95% were reached over 5 wt.% $\text{ZnCl}_2/\text{Al}_2\text{O}_3$ (No. II) catalyst at 180 °C (row 24, Table 5), and employing equimolar ratio of the reactants. Evidently, the materials based on commercial alumina (No. II) gave rise to the best performance both in case of non-impregnated and ZnCl_2 -impregnated materials.

The effect of feedstock molar ratio on the yield and selectivity was examined for 5 wt.% $\text{ZnCl}_2/\text{Al}_2\text{O}_3$ (No. II) catalyst at $T = 180$ °C only. It is revealed that in the case of small excess of isopropanol in the feedstock the yield decreased to ~78% whereas for the case of equimolar ratio it almost reached ~95% (row 25, Table 5). This could be explained by higher amounts of by-products, propene and diisopropyl ether, formed from excess of isopropanol. However, the possible reaction of diisopropyl ether with HCl towards isopropyl chloride does not lead to an increase of isopropyl chloride content in product mixture.

Commercial alumina No. I, impregnated with 5 wt.% ZnCl_2 was also found to be a good material leading to yield of around ~89–87%, at both of flow rates of HCl (rows 16 and 17, Table 5).

It should be noted that the impregnated 5 wt.% $\text{ZnCl}_2/\text{Al}_2\text{O}_3$ (No. I) catalyst gives rise to a significantly higher i-PrCl yield (~89%, row 16, Table 1) than the corresponding non-impregnated one (~25%, row 11, Table 5), at similar reaction conditions ($T = 180$ °C, feedstock molar ratio 1:1 and HCl flow rate of 10 mL/min). This result can confirm that the addition of ZnCl_2 (as a Lewis acid) to Lewis acidic γ -alumina is very important when aiming for the highest yield values, on par with the ethyl or methyl chlorides synthesis processes [20,40].

In case of the experiment over 5 wt.% $\text{ZnCl}_2/\text{Al}_2\text{O}_3$ (No. I) catalyst at reduced HCl flow rate the product yield slightly decreased (Table 5, row 17). On the contrary, in case of 2 wt.% $\text{ZnCl}_2/\text{Al}_2\text{O}_3$ (No. I) catalyst, decreasing the HCl flow rate down to 10 mL/min resulted in a slight increase in the yield values (70.5% and ~72%, respectively, rows 14 and 15, Table 5).

Finally, the best yield (in terms of both reactants) into isopropyl chloride (95.3%) was reached over 5 wt.% $\text{ZnCl}_2/\text{Al}_2\text{O}_3$ (No. II) catalyst at $T = 180$ °C, at a HCl flow rate of 20 mL/min and ni-PrOH:nHCl = 1:1. Catalysts, supported on commercial No. I and tailor-made alumina, 5 wt.% $\text{ZnCl}_2/\text{Al}_2\text{O}_3$ (No. I) and 5 wt.% $\text{ZnCl}_2/\text{Al}_2\text{O}_3$ (high porous) exhibited a bit lower but also high conversion values (89.2% and 89.6%, respectively) under identical conditions.

As shown in Fig. 3, depending on the amount of catalyst loading, different catalyst morphologies were found on the surface of carbon foam: film-like clusters at 2 wt.% ZnCl₂/C catalyst, a thin film at 5 wt.% ZnCl₂/C and a semi-thin film plus thick clusters at higher catalyst loading, i.e., 10 wt.% ZnCl₂/C material. Figs. 4 and 5 depict isopropyl chloride yield and selectivity over all groups of γ wt.% ZnCl₂/C catalysts. As shown in Table 5 (row 29), the maximum i-PrCl yield of only around ~75% could be reached over 5 wt.% ZnCl₂/C material which is much lower than in case of alumina. Also here, we can clearly show the dominant role of ZnCl₂ in terms of the reaction mechanism. As in case of alumina, increasing the ZnCl₂ percentage on the carbon support from 2 to 5 wt.% improves the yield from ~53% to ~75%, respectively (rows 27 and 29, Table 5). However, a further increase of the metal loading to 10 wt.% essentially reduced the catalyst performance. The plausible reasons could be the dramatically reduced surface area (rows 1–16, Table 1) due to pore blockage by excessive amounts of ZnCl₂ and the accumulation of ZnCl₂ to thick structures which subsequently reduced the active sites of ZnCl₂ catalyst. This could be explained by a shorter contact time of reactants inside the macroporous carbon-based catalyst at higher HCl flow rate.

Compared with alumina-based catalysts, the carbon-based catalysts were less active which could be explained by the natural higher catalytic activity of pure alumina substrate as it delivered i-PrCl yield up to ~60–78% (rows 2, 12 and 19, Table 5). Nevertheless, with the yield of ~75% and selectivity of ~91% (row 29, Table 5) for ZnCl₂ – decorated material, the carbon-based catalyst could be considered as a decent catalyst for the hydrochlorination of isopropanol to isopropyl chloride.

3.3. Acid–base titration data

An acid–base titration procedure was used to verify the accuracy of the calculations upon isopropyl chloride yield, obtained from GC data. The measurements were carried out for two experiments. The results are presented in Fig. 6 and in Table 6. It can be seen that in case of 5 wt. % ZnCl₂/Al₂O₃ (No. II) catalyst, the value obtained from titration data is in good agreement to that obtained from GC (Table 5). Larger discrepancy was observed in case of 5 wt.% ZnCl₂/Al₂O₃ (high porous) catalyst.

3.4. Products identification by GC-MS method

The results of GC–MS analysis are shown in Table 7 and in Fig. 7. As expected, the by-products are presented by species enlisted as follows: propylene, n-propyl chloride and diisopropyl ether. The presence of small amounts of propylene in the product mixture could be explained by an isopropanol dehydration side reaction over acid sites on the catalyst surface and the amounts of by-products depended on the catalyst [43–47]. Propylene formation occurs via intramolecular dehydration, whereas the formation of isopropyl ether, by intermolecular dehydration. The rate of isopropanol dehydration towards diisopropyl ether is much slower than those towards propene [46]. Moreover, the effect of the support is very important and using of γ - Al₂O₃ -based catalysts in isopropanol dehydration process leads to the essential increase of selectivity to ether in comparison to propylene step due to pore diameters in the range of Knudsen diffusion (1–100 nm) [48]. It can also explain the presence of n-propyl chloride which can be formed by an addition of HCl to propene, in the products mixture in amounts next to negligible.

3.5. Kinetic and reactor modelling

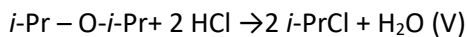
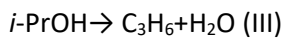
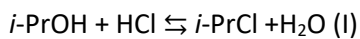
For the packed bed reactor, the ideal plug flow model is used:

$$\frac{dn_i}{dx} = r_i \rho_B \quad (1)$$

where n_i is molar flow of i-th component (mol/min), r_i is the component generation rates (mol/min) and ρ_B is the bulk density of the catalyst in the reactor ($w_{\text{cat}} \times m_{\text{cat}}/\text{volume}$), w_{cat} is the weight fraction of catalyst.

The effectiveness factor η was calculated to control whether the reaction of isopropanol hydrochlorination over porous catalysts is carrying out under kinetic or diffusion regime [49]. The Thiele modulus $\phi = \sqrt{(k/D_i)L}$, where L is particle radius (0.25 mm) and D_i is diffusion coefficient, was used to calculate the effectiveness factor. The diffusion coefficient D_i was calculated by the same procedure as in our previous work [22] and was obtained as $2.4 \times 10^{-6} \text{ m}^2/\text{s}$; approximated firstorder rate constant k was calculated as $1.68 \times 10^{-5} \text{ 1/min}$ at 175 °C. Thereby, the values of Thiele modulus $\phi = 0.0051$ and effectiveness factor $\eta = 1$ were obtained. These values calculated confirmed that the reaction of isopropanol hydrochlorination under given conditions was carried out under kinetic regime.

As this study is focused on catalyst testing there is limited data available for kinetic modelling and, therefore, we have limited the reaction kinetic study only to consider one reversible reaction producing directly to isopropyl chloride. To include the formation of i-PrCl through multiple routes and intermediates as in our previous work dealing with ethyl chloride synthesis [22] was not reasonable due to limited experimental information of the intermediates. Therefore, we only consider formation of i-PrCl with one reversible reaction and rate determining step (RDS) (Eq. (I) below).



The reaction rate for RDS is written as follows:

$$r_i = k_1 e^{-\frac{E_a}{R}(\frac{1}{T} - \frac{1}{T'})} \left(c_{i\text{-PrOH}} \times c_{\text{HCl}} - \frac{c_{i\text{-PrCl}} \times c_{\text{H}_2\text{O}}}{K_{\text{eq}}} \right)$$

For gas phase reactions the equilibrium constant can be calculated and we used the Gibbs equilibrium reactor model in the software Aspen Plus [50]. The equilibrium constants (K_{eq}) were calculated to be 382.2 at 150 °C, 139.9 at 170 °C, 122.7 at 180 °C and 314.5 at 200 °C.

Experiments over 2 wt.% $\text{ZnCl}_2/\text{Al}_2\text{O}_3$ (highly porous) catalyst were performed within a wider temperature range 150, 170, 180 and 200 °C so it was possible to estimate the activation energy for this dataset. The calculated value is $E_a = 57.6 \text{ kJ/mol}$. This E_a value was used also in the estimation of the rate constant for the experiments which performed over other catalysts within in a narrower temperature range (at 170 and 180 °C).

The software Modest was used for the modelling of the reaction kinetics [51]. This software solves the reactor model equations (system of ordinary differential equations) with the backward difference method and optimises the parameter values using a hybrid method involving Simplex and Levenberg-Marquardt methods.

The result of the parameter estimation, estimated rate constants are listed in Table 8. One can note that for some catalyst type the degree of explanation is not good mainly due to limited experimental data, whereas some of them are very good. One can make a comparison of the rates depending on the catalyst type.

The fit of model to experimental data is shown graphically (Figs. 8–14) with parity plots for all sets of data for each catalyst type and a plot showing the calculated molar flow profile of reactant (*i*-PrOH) and product (*i*-PrCl) as a function of reactor length coordinate for all datasets. The experimentally measured molar flow at the outlet of the reactor are indicated in the figure.

The E_a was calculated to be 57.6 kJ/mol which is significantly lower than for the liquid-phase reaction, described by Yang et al., where E_a value was found to be 72.3 kJ/mol [29].

Table 9 summarises the data of E_a , obtained in previous works for different short-chain alkyl chlorides. It is evident that the E_a values are decreasing from methyl to isopropyl chloride, with increasing of C atoms number in the chain of alcohols molecule.

3.6. Reaction mechanism

The proposed mechanism of isopropanol hydrochlorination reaction over alumina catalysts is presented on Scheme 1. The scheme describes four simultaneous processes of isopropyl chloride, propylene, *n*-propyl chloride and diisopropyl ether formation from isopropanol. In summary, the entire process can be presented as a combination of parallel reaction carried out on γ -alumina surface according to E1 and $S_{null}1$ mechanisms [52–62]. First, step 1 depicts the protonation stage – interaction of isopropanol with γ -alumina acid sites via OH-group [55,61] (which can also result in partial transformation of Lewis acid sites into Brønsted sites [62]), followed by dehydration step by E1 mechanism towards secondary propyl carbocation I (step 2). Further formation of main product, isopropyl chloride, is being carried out by $S_{null}1$ mechanism (step 3a). Beside, three reactions of formation diisopropyl ether (step 3b), *n*-propyl chloride (via formation of primary carbocation II and further $S_{null}1$ reaction towards isopropyl chloride, steps 3c and 3d) and propene (E1 mechanism, step 3e) can be listed as main side processes. The diisopropyl ether may be formed by $S_{null}1$ route but earlier it was reported also about alternative $S_{null}2$ mechanism [44,59]. However, actually both HCl and isopropanol are getting adsorbed at different active sites of the catalyst surface there by weakening the H-Cl and C-O bond (protonation of alcohol) in the first step, followed by dehydration (carbocation formation) and Cl addition (steps 2 and 3, respectively).

3.7. Long-time catalyst stability test

Catalyst lifetime is an important characteristic in terms of the industrial processes economy. In this work, a long-time test was performed for the catalyst selected as the best performing one, 5 wt.% ZnCl₂/Al₂O₃ (No. II). The experiment was carried out during 197 h and product samples were taken as follows: during the first 5 h the sampling time was 15 min; further, the samples were taken every 5 h (or 10 h overnight) during the rest of reaction time. Fig. 15 presents the results of *i*-PrCl yield over the catalyst selected at 180 °C. It is seen that the isopropyl chloride yield was high and remained so during all the testing time, with insignificant fluctuations. It was also evident that isopropyl chloride was the dominant component in the product mixture (Table 7). Thus, we can conclude that the catalytic material 5 wt.% ZnCl₂/Al₂O₃ (No. II) based on commercial alumina is a feasible choice upon synthesis of isopropyl chloride from isopropanol and HCl in gas phase under optimal reaction conditions.

4. Conclusions

Gas-phase reaction of isopropyl chloride synthesis from isopropyl alcohol and HCl was investigated over different catalysts. The maximum product selectivity 95.4% and *i*-PrCl yield 95.3% were achieved.

Two groups of catalyst materials such as alumina and carbon foam supports were studied. It was shown that commercial alumina, containing γ -Al₂O₃ phase was a better catalyst resulting in highest conversion

values, whereas both tailor made highly porous alumina and carbon foam supports exhibited much less catalytic performance. However, it was also shown that the slight increasing of ZnCl₂ loading up to 5 wt.% content in the alumina material led to significant increasing yields when both commercial and tailor-made alumina materials were employed.

All reaction products were identified and isopropyl chloride was always the dominant reaction product, complemented with minor byproducts such as propylene, n-propyl chloride and diisopropyl ether. Also, a plausible reaction network, represented by combination of the main reaction of isopropyl chloride formation and three side reactions was proposed.

The catalyst, supported on commercial alumina, 5 wt.% ZnCl₂/Al₂O₃ (No. II), was the best material, giving rise to the highest product yield during short and long testing time. It was shown that the yield and selectivity were stable during a very long time (197 h) thus rendering the materials suitable for continuous process of isopropyl chloride synthesis.

Acknowledgements

The Bio4Energy Programme and Kempe Foundations are gratefully acknowledged for financial support. This work is also part of the activities of the Johan Gadolin Process Chemistry Centre at Åbo Akademi University. The authors are grateful to Dr. Pasi Virtanen (Åbo Akademi, Finland) for his contribution in NH₃-TPD measurements.

Appendix A. Supplementary data

Supplementary data associated with this article can be found, in the online version, at <http://dx.doi.org/10.1016/j.apcata.2017.05.013>.

References

- [1] S. Haaf, H. Henrici, Refrigeration Technology, Ullmann's Encyclopedia of Industrial Chemistry; Wiley-VCH Verlag GmbH & Co. KGaA, 2000 DOI: 10.1002/14356007.b03_19.
- [2] Summary of Emissions Associated with Sources of Ethyl Chloride; EPA-450/3-88-005; Emissions Standards Division, Office of Air and Radiation, Office of Air Quality Planning and Standards, U.S. Environmental Protection Agency: Research Triangle Park, NC, June 1988, pp 3.1–3.16.
- [3] J.E. Elam, M.L. Newhouse, British Med. J. 1 (4696) (1951) 13–14.
- [4] T.J.C. MacDonald, Brit. J. Anaesth. 22 (2) (1950) 92–101.
- [5] J.D. Holbrey, K.R. Seddon, R. Wareing, Green Chem. 3 (2001) 33–36.
- [6] A.B. Savage, A.E. Young, A.T. Maser, In: Cellulose and Cellulose Derivatives; Ott, E., Ed.; Interscience: New York; 913.
- [7] W. Gerhartz (exec ed.). Ullmann's Encyclopedia of Industrial Chemistry. 5th ed. Vol A1. VCH Publishers: Deerfield Beach, FL, 1985 to Present, p. VA6 310.
- [8] M.F. Nagiev, R.A. Makhmudzade, Zh.I. Kashkai, Azerb. Him. Zhurn. 6 (1968) 25–32.
- [9] M.F. Nagiev, Zh.I. Kashkai, R.A. Makhmudzade, Azerb. Him. Zhurn. 4 (1969) 3–7.

- [10] M.F. Nagiev, Zh.I. Kashkai, R.A. Makhmudzade, *Azerb. Him. Zhurn.* 6 (1969) 27–32.
- [11] H. Buc, U.S. Patent 1436377, Standard Development, 1922.
- [12] R. Herrmann, U.S. Patent 4073816, Deutsche Texaco Aktiengesellschaft, 1978.
- [13] J. Grolig, M. Martin, G. Scharfe, U.S. Patent 4009216, Bayer Aktiengesellschaft, Leverkusen, Germany, 1977.
- [14] R.L. Klausmeyer, D.E. Brummond, U.S. Patent 6617479 B1, Vulcan Chemical division of Vulcan Materials Company, Birmingham, AL (US), 2003.
- [15] T. Matsumoto, T. Nakano, Y. Yokoyama, Y. Makiguchi, U.S. Patent 7078576 B2, Kashima Chemical Company, Limited Kashima-gun (JP); Asahi Glass company, limited, Tokyo (JP), 2006.
- [16] E.L. Mainz, R.L. Wilson, J.L. Dawkins, J.M. Nyberg, U.S. Patent 2004/0204619 A1, Vulcan Chemicals a Business Group of Vulcan Materials Company, 2004.
- [17] D. Chang, D.T. Allen, *J. Ind. Ecol.* 1 (2) (1997) 111–134.
- [18] A.M. Becerra, A.E. Castro Luna, D.E. Ardisson, M.I. Ponzi, *Ind. Eng. Chem. Res.* 31 (1992) 1040–1045.
- [19] M.S. Thyagarajan, R. Kumar, N.R. Kuloor, *I & EC Proc. Des. Dev.* 5 (3) (1966) 209–213.
- [20] N. Bukhanko, A. Samikannu, W. Larsson, A. Shchukarev, A.-R. Leino, K. Kordas, J. Wärnå, J.-P. Mikkola, *ACS Sustainable Chem. Eng.* 1 (2013) 883–893.
- [21] S.A. Schmidt, N. Kumar, A. Reinsdorf, K. Eränen, J. Wärnå, D.Yu. Murzin, T. Salmi, *Chem. Eng. Sci.* 95 (2013) 232–245.
- [22] N. Bukhanko, J. Wärnå, A. Samikannu, J.-P. Mikkola, *Chem. Eng. Sci.* 142 (2016) 310–317.
- [23] S.A. Schmidt, Q. Balme, N. Gemo, N. Kumar, K. Eränen, D.Yu. Murzin, T. Salmi, *Chem. Eng. Sci.* 134 (2015) 681–693.
- [24] Y. Soma, K. Inokuma, T. Tanaka, C. Ogino, A. Kondo, M. Okamoto, T. Hanai, *J. Biosci. Bioeng.* 114 (1) (2012) 80–85.
- [25] K. Inokuma, J.C. Liao, M. Okamoto, T. Hanai, *J. Biosci. Bioeng.* 110 (6) (2010) 696–701.
- [26] V. Sanchez i Nogue, B.A. Black, D. Salvachua, E.M. Karp, G.T. Beckham, *Recent Advances in Fermentation Technology (RAFT 11) Workshop*, November 8–11, Hilton Clearwater Beach Hotel, Clearwater Beach, FL, USA, 2015.
- [27] <http://www.bioisopropanol.com>.
- [28] P. Tundo, P. Venturello, E. Angeletti, *J. Chem. Soc., Perkin Trans. 1* (1987) 2157–2158.
- [29] E. Yang, J. Hao, Y. Wang, Y. Cao, Y. Zhang, *Speciality Petrochemicals* 1 (2001) 16–19.
- [30] B. Nkosi, M.D. Adams, N.J. Coville, G.J. Hutchings, *J. Catal.* 128 (2) (1991) 378–386.
- [31] M. Conte, A.F. Carley, G.J. Hutchings, *Catal. Lett.* 124 (3–4) (2008) 165–167.
- [32] Y. Dong, W. Li, Z. Yan, J. Zhang, *Catal. Sci. Technol.* (2016), <http://dx.doi.org/10.1039/c6cy01241h>.

- [33] J. Zhao, J. Xu, J. Xu, J. Ni, T. Zhang, X. Xu, X. Li, *Chem. Plus Chem.* 80 (1) (2015) 196–201.
- [34] T.N. Pham, A. Samikannu, J. Kukkola, A.-R. Rautio, O. Pitkaenen, A. Dombovari, G.S. Lorite, T. Sipola, G. Toth, M. Mohl, J.-P. Mikkola, K. Kordas, *Sci. Rep.* 4 (2014) 6933
<http://www.nature.com/srep/2014/141106/srep06933/full/srep06933.html>.
- [35] T.N. Pham, A. Samikannu, A.-R. Rautio, K.L. Juhasz, Z. Konya, J. Wärnä, K. Kordas, J.-P. Mikkola, *Top. Catal.* 59 (13) (2016) 1165–1177.
- [36] M.M. Hossain, *Can. J. Chem. Eng.* 9999 (2011) 1–10.
- [37] F. Lónyi, J. Valyon, *Microporous Mesoporous Mater.* 47 (2001) 293–301.
- [38] M.R. Gafurov, I.N. Mukhambetov, B.V. Yavkin, G.V. Mamin, A.A. Lamberov, S.B. Orlinskii, *J. Phys. Chem. C* 119 (2015) 27410–27415.
- [39] G.N. Lysenko, P.P. Mardilovich, A.I. Trokhimetz, *React. Kinet. Catal. Lett.* 31 (1986) 377–381.
- [40] E.B. Svetlanov, R.M. Flid, D.A. Gareeva, *Russ. J. Phys. Chem.* 40 (1966) 2302–2308.
- [41] S. Srinivasan, C.R. Narayanan, A. Biaglow, R. Gorte, A.K. Datye, *Appl. Catal. A: General* 132 (1995) 271–287.
- [42] C.R. Narayanan, S. Srinivasan, A.K. Datye, R. Gorte, A. Biaglow, *J. Catal.* 138 (2) (1992) 659–674.
- [43] J. Bedia, R. Ruiz-Rosas, J. Rodriguez-Mirasol, T. Cordero, *J. Catal.* 271 (1) (2010) 33–42.
- [44] K. Larmier, C. Chizallet, N. Cadran, S. Maury, J. Abboud, A.-F. Lamic-Humblot, E. Marceau, H. Lauron-Pernot, *ACS Catal.* 5 (7) (2015) 4423–4437.
- [45] K. Larmier, A. Nicolle, C. Chizallet, N. Cadran, S. Maury, A.-F. Lamic-Humblot, E. Marceau, H. Lauron-Pernot, *ACS Catal.* 6 (2016) 1905–1920.
- [46] A. Rouge, B. Spoetzl, K. Gebauer, R. Schenk, A. Renken, *Chem. Eng. Sci.* 56 (2001) 1419–1427.
- [47] K. Koehloefl, I.-Z. Knozinger, *Proc. Fifth Int. Congr. Catal.* (1973), p. 1171.
- [48] A.S. Araujo, M.J.B. Souza, V.J. Fernandes Jr., J.C. Diniz, *React. Kinet. Catal. Lett.* 66 (1) (1999) 141–146.
- [49] T.O. Salmi, J.-P. Mikkola, J. Wärnä, *Chemical Reaction Engineering and Reactor Technology*, CRC Press, Taylor & Francis Group, Boca Raton – London – New York, 2010.
- [50] <http://www.aspentech.com>.
- [51] H. Haario, *MODEST User's guide*, Profmath Oy. Hels., 2007.
- [52] H. Knözinger, R. Köhne, *J. Catal.* 5 (2) (1966) 264–270.
- [53] H. Knözinger, H. Bühl, E. Ress, *J. Catal.* 12 (2) (1968) 121–128.
- [54] P.A. Clayborne, T.C. Nelson, T.C. DeVore, *Appl. Catal. A: General* 257 (2004) 225–233.
- [55] S. Cai, K. Sohlberg, *J. Mol. Catal. A: Chem.* 193 (2003) 157–164.
- [56] S. Roy, G. Mpourmpakis, D.-Y. Hong, D.G. Vlachos, A. Bhan, R.J. Gorte, *ACS Catal.* 2 (2012) 1846–1853.
- [57] P. Kostestkyy, J. Yu, R.J. Gorte, G. Mpourmpakis, *Catal. Sci. Technol.* 4 (2014) 3861–3869.

- [58] J.H. Kwak, D. Mei, C.H.F. Peden, R. Rousseau, J. Szanyi, Catal. Lett. 141 (2011) 649–655.
- [59] B. Shi, B.H. Davis, J. Catal. 157 (1995) 359–367.
- [60] J.A. Wang, X. Bokhimi, O. Novaro, T. Lopez, F. Tzompantzi, R. Gomez, J. Navarrete, M.E. Llanos, E. Lopez-Salinas, J. Mol. Catal. A: Chem. 137 (1999) 239–252.
- [61] G. Feng, C.-F. Huo, C.-M. Deng, L. Huang, Y.-W. Li, J. Wang, H. Jiao, J. Mol. Catal. A: Chem. 304 (2009) 58–64.
- [62] C. Lahousse, F. Maugé, J. Bachelier, J.-C. Lavalley, J. Chem. Soc., Faraday Trans. 91 (1995) 2907–2912.

TABLES AND FIGURES

TABLE 1. B.E.T. surface area, pore size and pore volume data for the alumina-based and carbon-based catalysts.

N	Catalyst	Surface area (m ² /g)		Pore size (nm)		Pore volume (cm ³ /g)	
		Fresh	Spent	Fresh	Spent	Fresh	Spent
Al ₂ O ₃ (highly porous) supported materials							
1	Al ₂ O ₃ (highly porous)	429.8	405.5	13.1	17.3	1.4	1.8
2	2 wt.% ZnCl ₂ /Al ₂ O ₃ (highly porous)	418.3	341.0	17.5	18.3	1.8	1.6
3	5 wt.% ZnCl ₂ /Al ₂ O ₃ (highly porous)	438.1	343.5	21.8	24.3	2.4	2.1
Al ₂ O ₃ (No. I) supported materials							
4	Al ₂ O ₃ (No. I)	335.5	234.6	4.7	7.9	0.4	0.5
5	2 wt.% ZnCl ₂ /Al ₂ O ₃ (No. I)	317.4	199.1	4.5	7.3	0.4	0.4
6	2 wt.% ZnCl ₂ /Al ₂ O ₃ (No. I)	317.4	220.5	4.5	5.6	0.4	0.3
7	5 wt.% ZnCl ₂ /Al ₂ O ₃ (No. I)	248.5	180.2	5.6	7.9	0.3	0.4
Al ₂ O ₃ (No. II) supported materials							
8	Al ₂ O ₃ (No. II)	323.2	231.3	5.0	5.9	0.4	0.3
9	2 wt.% ZnCl ₂ /Al ₂ O ₃ (No. II)	302.8	196.9	5.0	6.7	0.4	0.3
10	2 wt.% ZnCl ₂ /Al ₂ O ₃ (No. II)	302.8	197.5	5.0	6.7	0.4	0.3
11	5 wt.% ZnCl ₂ /Al ₂ O ₃ (No. II)	254.5	176.3	5.5	11.8	0.3	0.5
12	5 wt.% ZnCl ₂ /Al ₂ O ₃ (No. II)	254.5	212.3	5.5	8.7	0.3	0.5
13	5 wt.% ZnCl ₂ /Al ₂ O ₃ (No. II)	254.5	140.6	5.5	11.0	0.3	0.4
C-supported materials							
14	2 wt.% ZnCl ₂ /C	322.0	4.5	14.9	40.9	1.2	0.04
15	5 wt.% ZnCl ₂ /C	172.0	4.5	2.6	11.8	0.1	0.01
16	10 wt.% ZnCl ₂ /C	4.0	2.8	68.0	62.9	0.06	0.04
Reaction conditions: T =180 °C, HCl flow rate 10 mL/min, n _{i-PrOH} :n _{HCl} = 1:1, t= 300 min (Rows 1,3,4,5,7,8,9,14,15,16).							
Reaction conditions: T =150 °C, HCl flow rate 20 mL/min, n _{i-PrOH} :n _{HCl} = 1:1, t= 366 min (Row 2).							
Reaction conditions: T =180 °C, HCl flow rate 20 mL/min, n _{i-PrOH} :n _{HCl} = 1:1, t= 300 min (Rows 6,10,12).							
Reaction conditions: T =170 °C, HCl flow rate 20 mL/min, n _{i-PrOH} :n _{HCl} = 1:1, t= 309 min (Row 11).							
Reaction conditions: T =180 °C, HCl flow rate 10 mL/min, n _{i-PrOH} :n _{HCl} = 1:1, t= 11825 min (Row 13).							

TABLE 2. Atomic ratios (XPS data) at the surface of catalysts before and after the reaction.

N		Catalyst	Al-OH/Al-O	Cl/Al	Cl/Zn	Al/Zn
1	Al ₂ O ₃ (highly porous)	Fresh	0.05	–	–	–
		Spent*	0.73	0.13	–	–
2	2 wt.% ZnCl ₂ /Al ₂ O ₃ (highly porous)	Fresh	0.35	0.02	0.98	80
		Spent	0.40	0.12	4.70	83
3	2 wt.% ZnCl ₂ /Al ₂ O ₃ (No. I)	Fresh	1.09	0.04	3.36	82
		Spent	1.25	2.23	2.64	103
4	2 wt.% ZnCl ₂ /Al ₂ O ₃ (No. II)	Fresh	0.94	0.04	2.69	64
		Spent*	1.28	0.08	2.98	102
		Spent**	0.72	0.07	2.10	72
5	5 wt.% ZnCl ₂ /Al ₂ O ₃ (highly porous)	Fresh	0.50	0.05	1.83	29
		Spent	0.51	0.17	5.51	33
6	5 wt.% ZnCl ₂ /Al ₂ O ₃ (No. I)	Fresh	0.48	0.05	1.45	27
		Spent	0.47	0.12	3.72	32
7	5 wt.% ZnCl ₂ /Al ₂ O ₃ (No. II)	Fresh	0.50	0.05	1.45	27
		Spent*	0.48	0.10	3.34	33.5
		Spent**	0.48	0.11	3.62	33
Reaction conditions: T =180 °C, flow rate HCl =20 mL/min, n _{i-PrOH} :n _{HCl} = 1:1, t = 300 min (Row 1).						
Reaction conditions: T =150 °C, flow rate HCl =20 mL/min, n _{i-PrOH} :n _{HCl} = 1:1, t = 300 min (Row 2).						
Reaction conditions: T =180 °C, flow rate HCl =20 mL/min, n _{i-PrOH} :n _{HCl} = 1:1, t = 300 min (Rows 3, 4*, 7*).						
Reaction conditions: T =170 °C, flow rate HCl =20 mL/min, n _{i-PrOH} :n _{HCl} = 1:1, t = 300 min (Row 4**).						
Reaction conditions: T = 180 °C, flow rate HCl = 12.314 mL/min, n _{i-PrOH} :n _{HCl} = 1:1, t = 11825 min (Row 7**).						
Reaction conditions: T =180 °C, flow rate HCl =10 mL/min, n _{i-PrOH} :n _{HCl} = 1:1, t = 300 min (Rows 5, 6).						

TABLE 3. Atomic ratios at the surface of the carbon-catalysts-group before and after the reaction.

Catalyst	Cl/Zn	(C+N)/Zn*
5 wt.% ZnCl ₂ /C fresh	0.49	90.2
5 wt.% ZnCl ₂ /C spent**	26.25	754.6
* Carbon foam, produced from melamine, consists of C and N.		
** Reaction conditions: T = 180 °C, flow rate HCl= 10 mL/min, n _{i-PrOH} :n _{HCl} =1:1, t = 300 min.		

TABLE 4. Total acidity values, calculated from NH₃-TPD data for alumina-based catalysts.

N	Catalyst	T(°C)	Peak area	Acidity (mmol/g)	Total acidity (mmol/g)
<i>Al₂O₃ (high porous) – supported materials</i>					
1	Al ₂ O ₃ (high porous)	206	570	27	27
2	2 wt.% ZnCl ₂ /Al ₂ O ₃ (high porous)	231	435	21	21
3	5 wt.% ZnCl ₂ /Al ₂ O ₃ (high porous)	285	599	28	28
<i>Al₂O₃ (No. I) – supported materials</i>					
4	Al ₂ O ₃ (No. I)	222	90	4	25
		268	101	5	
		441	334	16	
5	2 wt.% ZnCl ₂ /Al ₂ O ₃ (No. I)	267	167	8	26
		445	376	18	
6	5 wt.% ZnCl ₂ /Al ₂ O ₃ (No. I)	330	212	10	27
		545	368	17	
<i>Al₂O₃ (No. II) – supported materials</i>					
7	Al ₂ O ₃ (No. 2)	229	167	8	20
		458	260	12	
8	2 wt.% ZnCl ₂ /Al ₂ O ₃ (No. II)	254	204	10	22
		472	250	12	
9	5 wt.% ZnCl ₂ /Al ₂ O ₃ (No. II)	276	232	11	23
		516	260	12	

TABLE 5. Isopropyl chloride yield and selectivity data for experiments over different catalysts and reactions conditions.

N	Catalyst	T (°C)	HCl flow rate (mL / min)	n _{i-PrOH} :n _{HCl}	Y _{i-PrCl} (%)	S _{i-PrCl} (%)
<i>Al₂O₃ (highly porous) supported materials</i>						
1	Al ₂ O ₃ (highly porous)	180	20	1:1	71.4	91.5
2	Al ₂ O ₃ (highly porous)	180	10	1:1	61.6	90.4
3	Al ₂ O ₃ (highly porous)	170	20	1:1	62.5	91.3
4	Al ₂ O ₃ (highly porous)	200	20	1:1	40.7	81.3
5	2 wt.% ZnCl ₂ /Al ₂ O ₃ (highly porous)	150	20	1:1	36.1	88.2
6	2 wt.% ZnCl ₂ /Al ₂ O ₃ (highly porous)	170	20	1:1	47.7	92.2
7 ^a	2 wt.% ZnCl ₂ /Al ₂ O ₃ (highly porous)	180	20	1:1	48.3	89.8
8	2 wt.% ZnCl ₂ /Al ₂ O ₃ (highly porous)	180	20	1:1	61.9	92.9
9	5 wt.% ZnCl ₂ /Al ₂ O ₃ (highly porous)	180	20	1:1	89.6	93.7
10	5 wt.% ZnCl ₂ /Al ₂ O ₃ (highly porous)	180	10	1:1	79.8	92.7
<i>Al₂O₃ (No. I) supported materials</i>						
11	Al ₂ O ₃ (No. I)	180	20	1:1	24.6	69.3
12	Al ₂ O ₃ (No. I)	180	10	1:1	78.2	90.2
13	2 wt.% ZnCl ₂ /Al ₂ O ₃ (No. I)	170	20	1:1	48.6	90.8
14	2 wt.% ZnCl ₂ /Al ₂ O ₃ (No. I)	180	20	1:1	70.5	90.9
15	2 wt.% ZnCl ₂ /Al ₂ O ₃ (No. I)	180	10	1:1	71.6	89.9
16 ^a	5 wt.% ZnCl ₂ /Al ₂ O ₃ (No. I)	180	20	1:1	89.2	91.8
17	5 wt.% ZnCl ₂ /Al ₂ O ₃ (No. I)	180	10	1:1	87.3	90.7
<i>Al₂O₃ (No. II) supported materials</i>						
18	Al ₂ O ₃ (No. II)	180	20	1:1	65.4	90.9
19	Al ₂ O ₃ (No. II)	180	10	1:1	62.2	89.1
20	2 wt.% ZnCl ₂ /Al ₂ O ₃ (No. II)	170	20	1:1	74.4	90.7
21	2 wt.% ZnCl ₂ /Al ₂ O ₃ (No. II)	180	20	1:1	81.7	91.0
22	2 wt.% ZnCl ₂ /Al ₂ O ₃ (No. II)	180	10	1:1	80.7	91.3
23	5 wt.% ZnCl ₂ /Al ₂ O ₃ (No. II)	170	20	1:1	90.5	93.5
24a	5 wt.% ZnCl ₂ /Al ₂ O ₃ (No. II)	180	20	1:1	95.3	95.4
25	5 wt.% ZnCl ₂ /Al ₂ O ₃ (No. II)	180	20	1.05:1	77.8	92.5
26	5 wt.% ZnCl ₂ /Al ₂ O ₃ (No. II)	180	10	1:1	68.1	90.6
<i>Carbon supported materials</i>						
27	2 wt.% ZnCl ₂ /C	180	10	1:1	52.7	86.7
28	5 wt.% ZnCl ₂ /C	180	20	1:1	30.2	85.5
29	5 wt.% ZnCl ₂ /C	180	10	1:1	74.6	91.2
30	10 wt.% ZnCl ₂ /C	180	10	1:1	54.0	90.0

^aReaction time: t = 692 min (Row 7), t = 1863 min (Row 16), t = 1592 min (Row 24).

TABLE 6. Values of isopropyl chloride yield, obtained from GC and titration data.

Catalyst	HCl conversion			
	GC data		Titration data	
	Y_{i-PrCl} (%)	Standard deviation	Y_{i-PrCl} (%)	Standard deviation
5 wt.% ZnCl ₂ /Al ₂ O ₃ (No. II)	71.9	0.1	72.3	2.6
5 wt.% ZnCl ₂ /Al ₂ O ₃ (highly porous)	79.8	0.1	68.0	2.9

TABLE 7. The composition of product mixture, determined from GC-MS data.

N	Component	R.T. (min)	TIC peak area% of total	Probability (%)
1	Propene	1.60	2.96	72.1
2	Isopropyl chloride	2.39	94.70	92.7
3	n-Propyl chloride	2.62	0.06	60.6
4	Isopropyl alcohol	2.73	1.49	74.4
5	Diisopropyl ether	3.91	0.80	74.4

TABLE 8. The parameter estimation data and estimated rate constants.

Catalyst	k Ea	Std error %	Degree of explanation %	Catalyst weight fraction
5 wt.% ZnCl ₂ /Al ₂ O ₃ (No. I)	3.37E-06	17.8	87.2	0.02–0.05
5 wt.% ZnCl ₂ /Al ₂ O ₃ (No. II)	1.3E-04	Large	98.9	0.02–0.05
5 wt.% ZnCl ₂ /Al ₂ O ₃ (high porous)	1.84E-06	2.2	97.1	0.02
	57.6	4.3		
10 wt.% ZnCl ₂ /C	2.08E-07	17	90	0.02–0.05
Al ₂ O ₃ (No. I)	1.85E-06	30.4	71.4	1
Al ₂ O ₃ (No. II)	2.16E-08	1.1	99.8	1
Al ₂ O ₃ (high porous)	4.49E-08	10.8	65.5	1

$E_a = 57.6$ kJ/mol; $T_{mean} = 175$ °C; unit for the rate constant k (m³/mol•min).

TABLE 9. Comparison data for E_a of primary alcohols catalytic hydrochlorination reaction.

Alkyl chloride	E_a (kJ/mol)	Reference
Methyl chloride	108	Schmidt et al., 2013 [21]
	80	Thyagarajan et al., 1966 [19]
Ethyl chloride	78.9	Schmidt et al., 2015 [23]
80;	80; 71	Bukhanko et al., 2013 [20]
	45; 95; 68; 100	Bukhanko et al., 2016 [22]
Isopropyl chloride	57.6	Present work
	72.3	Yang et al., 2001 [29] *

* The reaction of isopropanol hydrochlorination was performed in liquid phase.

Fig. 1. Transmission electron microscopy images of fresh and spent* 5 wt.% ZnCl₂/Al₂O₃ catalysts: a) 5 wt.% ZnCl₂/Al₂O₃ (N I) fresh, b) 5 wt.% ZnCl₂/Al₂O₃ (N I) spent, c) 5 wt.% ZnCl₂/Al₂O₃ (N II) fresh, d, e) 5 wt.% ZnCl₂/Al₂O₃ (N II) spent, f) 5 wt.% ZnCl₂/Al₂O₃ (high porous) fresh, g) 5 wt.% ZnCl₂/Al₂O₃ (high porous) spent. *The reaction conditions for spent materials: b, g) T = 180 °C, flow rate HCl = 10 mL/min, ni-PrOH: nHCl = 1:1, t = 300 min. d) T = 180 °C, flow rate HCl = 20 mL/min, ni-PrOH: nHCl = 1.05:1, t = 300 min. e) T = 180 °C, flow rate HCl = 10 mL/min, ni-PrOH: nHCl = 1:1, t = 11825 min.

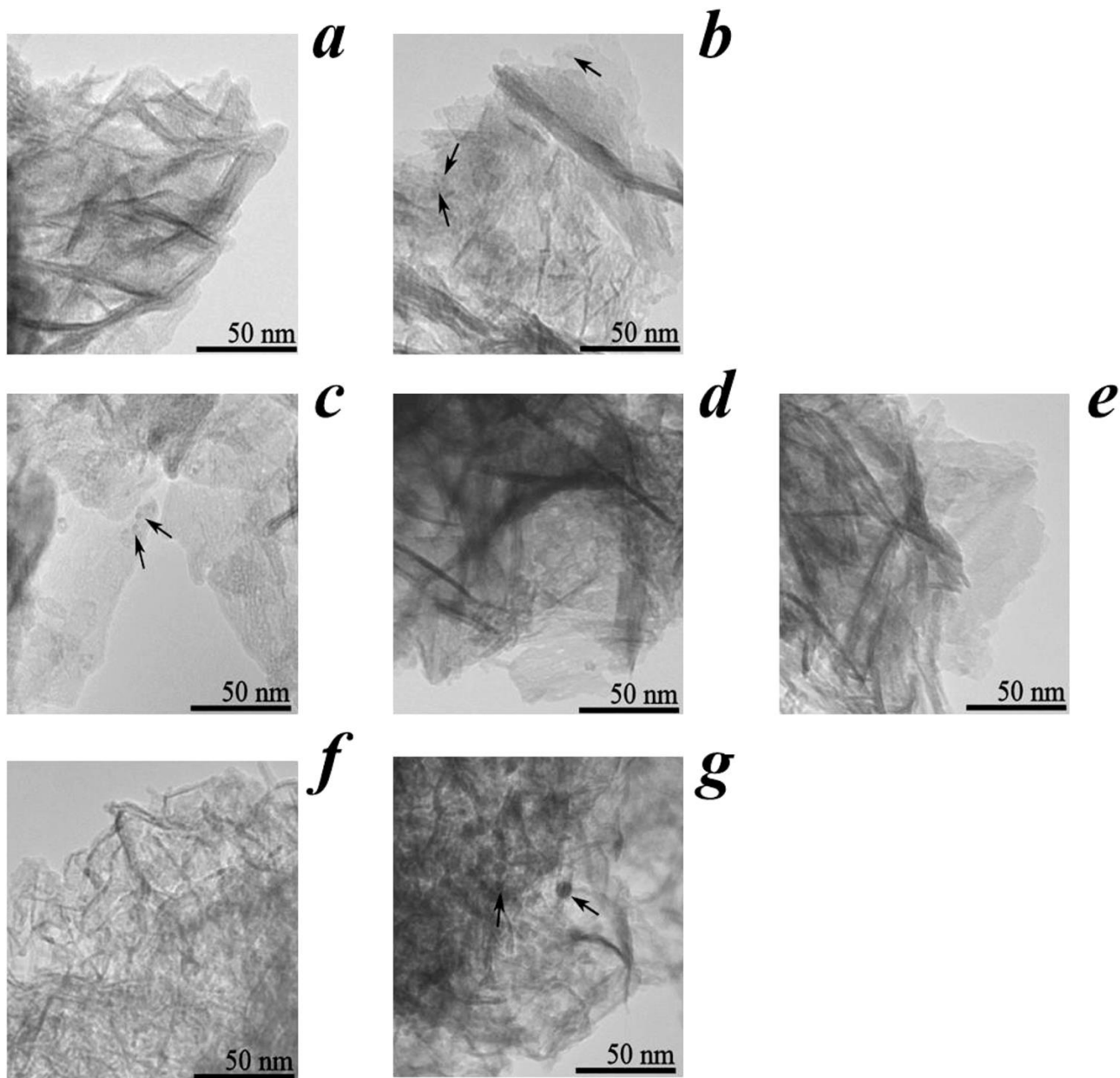


Fig. 2. Summary of NH₃-TPD profiles for alumina-based catalysts.

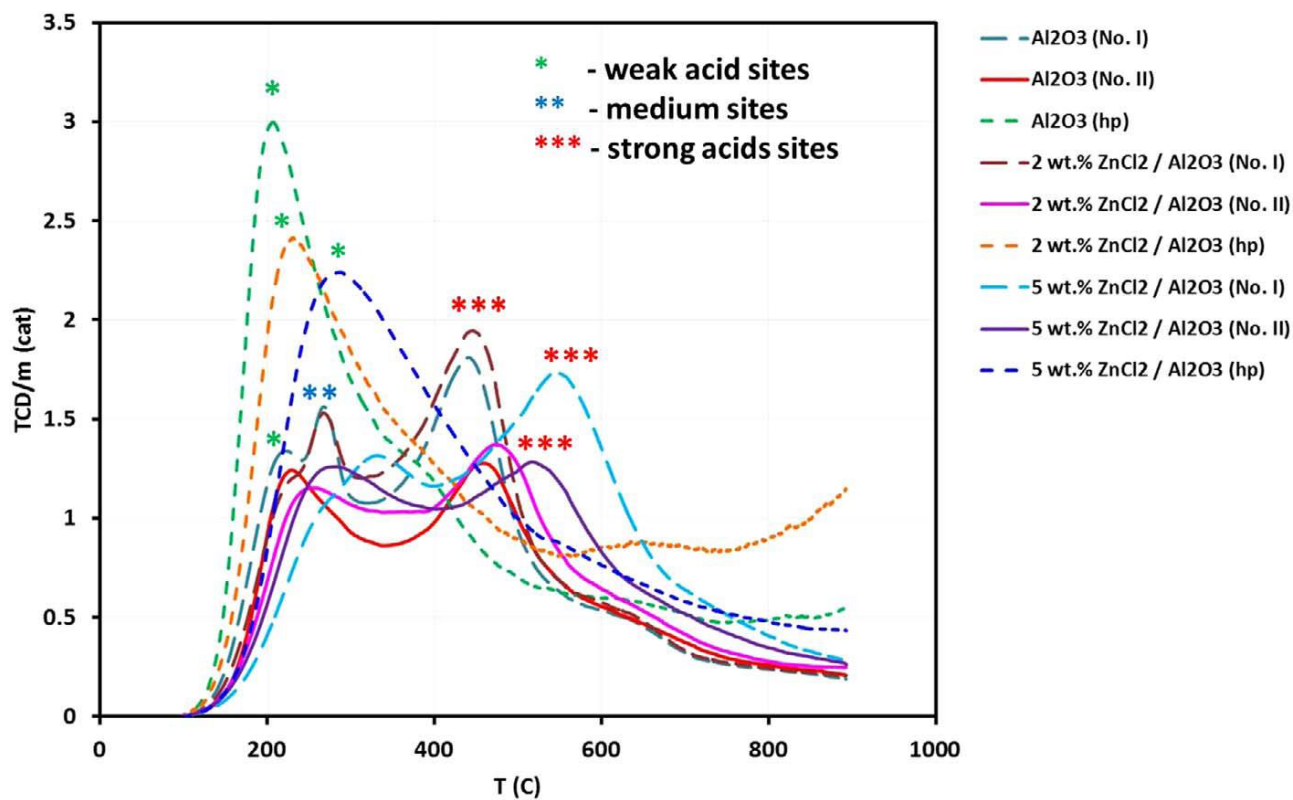


Fig. 3. SEM images of γ wt.% ZnCl₂/C catalysts: $\gamma=2$ wt.% (a), $\gamma=5$ wt.% (b) and $\gamma=10$ wt.% (c) catalyst loading and TEM image of spent 5 wt.% ZnCl₂/C catalyst (d). Reaction conditions: T = 180 °C, flow rate of HCl = 10 mL/min, n_{i-PrOH}:n_{HCl} = 1:1.

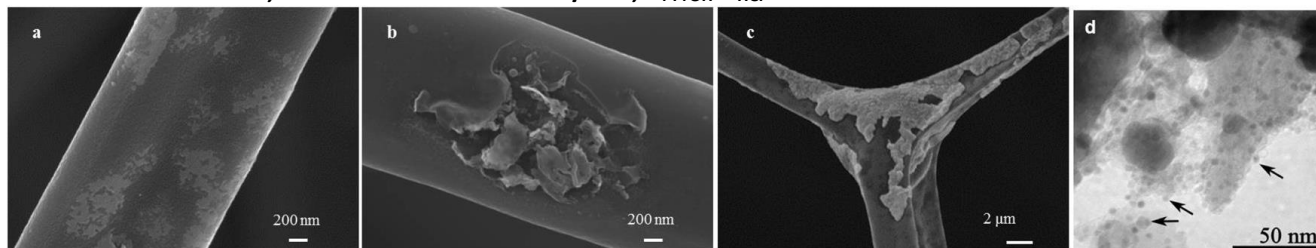


Fig. 4. Values of *i*-PrCl yield and selectivity over carbon-based catalysts γ wt.% ZnCl₂/C ($\gamma = 2, 5, 10$). Reaction conditions: T = 180 °C, flow rate of HCl = 10 mL/min (*=20 mL/min), $n_{i-PrOH}:n_{HCl} = 1:1$.

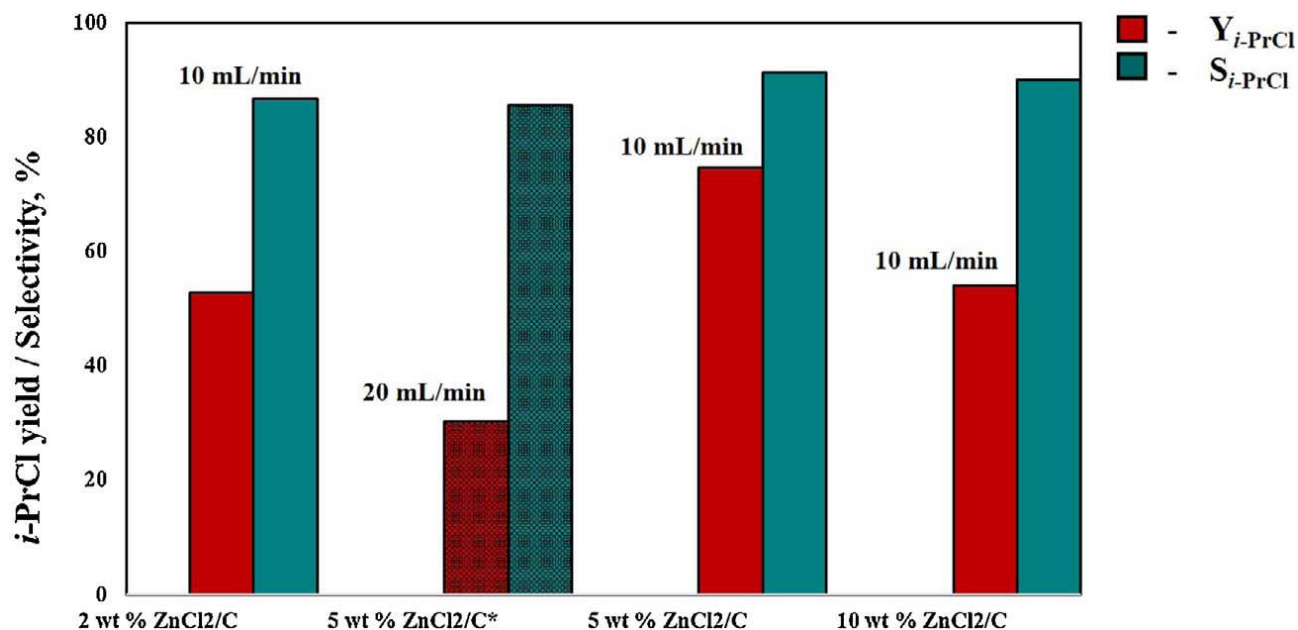


Fig. 5. Values of *i*-PrCl yield (a) and selectivity (b) over γ wt.% ZnCl₂/C catalysts at different feedstock flow rates. Reaction conditions: T = 180 °C, $n_{i-PrOH}:n_{HCl} = 1:1$.

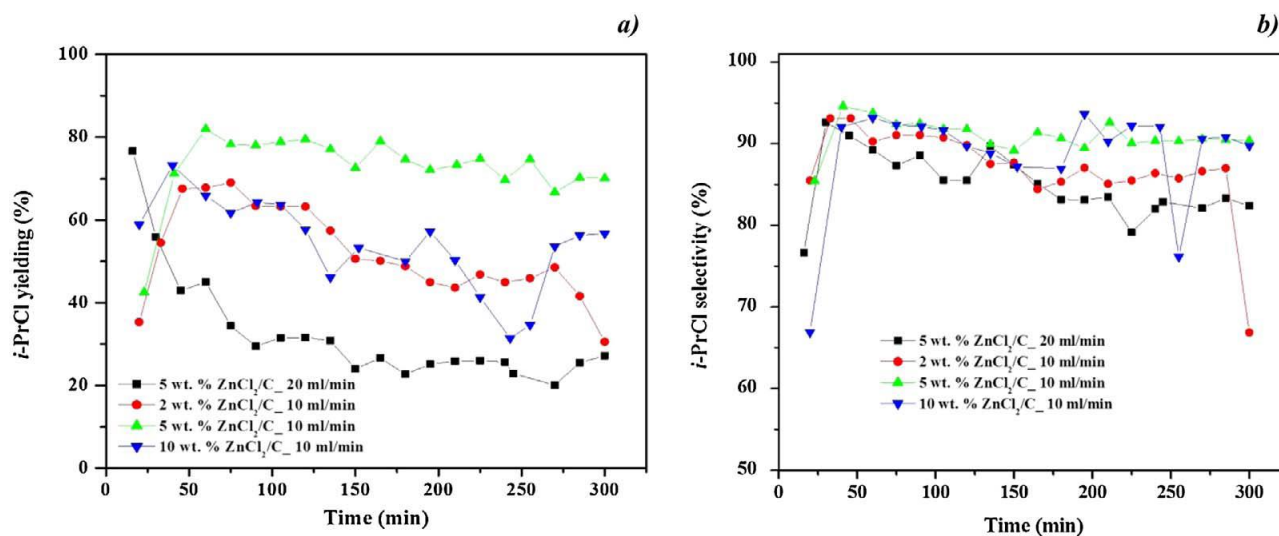


Fig. 6. Values of i-PrCl yield, obtained from acid–base titration data. The titration procedure was performed over 5 wt.% ZnCl₂/Al₂O₃ (No. II) after 197 h of reaction time (a) and over 5 wt.% ZnCl₂/Al₂O₃ (high porosity) catalyst after 5 h (b).

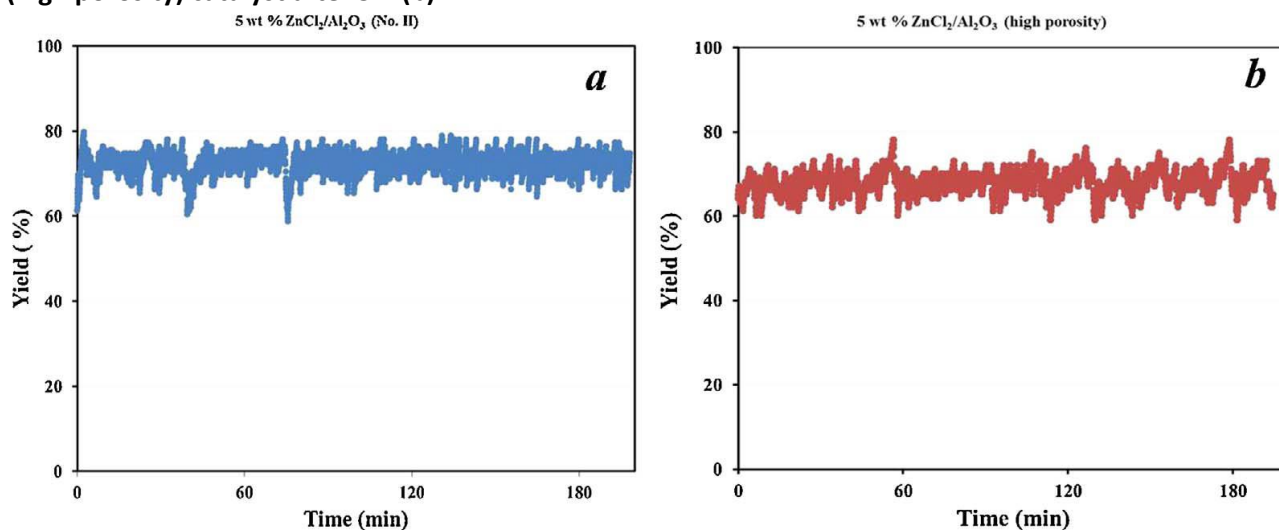


Fig. 7. Components of products mixture, produced over 5 wt.% ZnCl₂/Al₂O₃ (No. II) catalyst, determined by GC-MS data. The reaction conditions: T = 180 °C, n_{i-PROH}:n_{HCl} = 1:1, t = 11825 min.

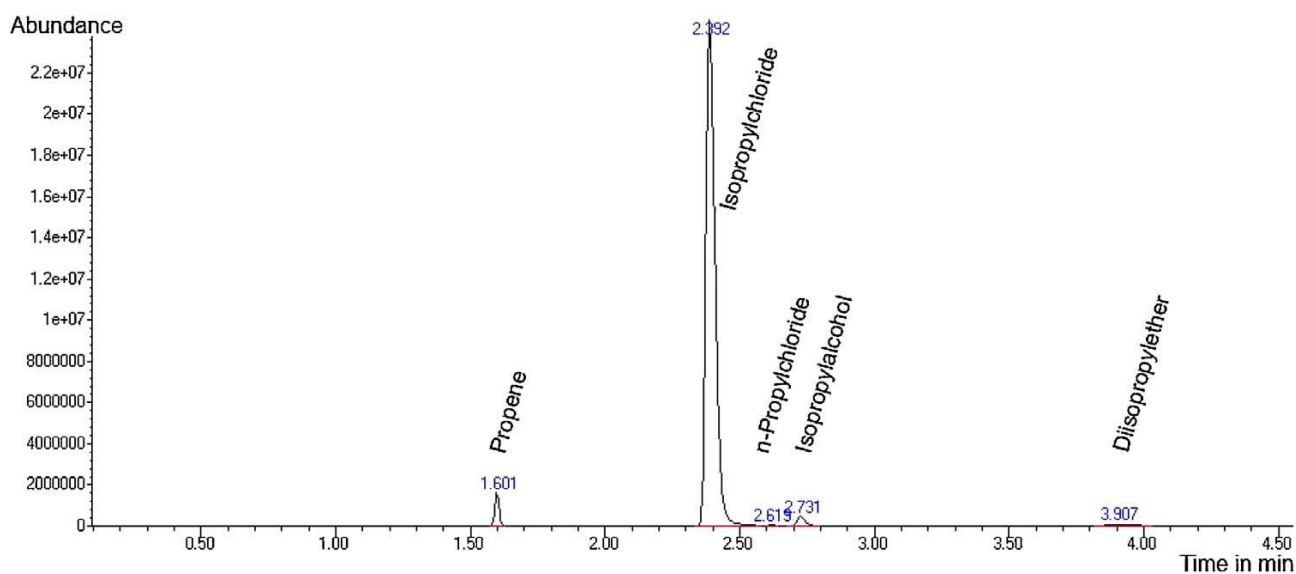


Fig. 8. Parity plot (a) and calculated molar flows inside the reactor tube over 5 wt.% ZnCl₂/Al₂O₃ (highly porous) catalyst (b). The reaction conditions: T =180 °C, n_{i-PrOH}:n_{HCl} =1:1.

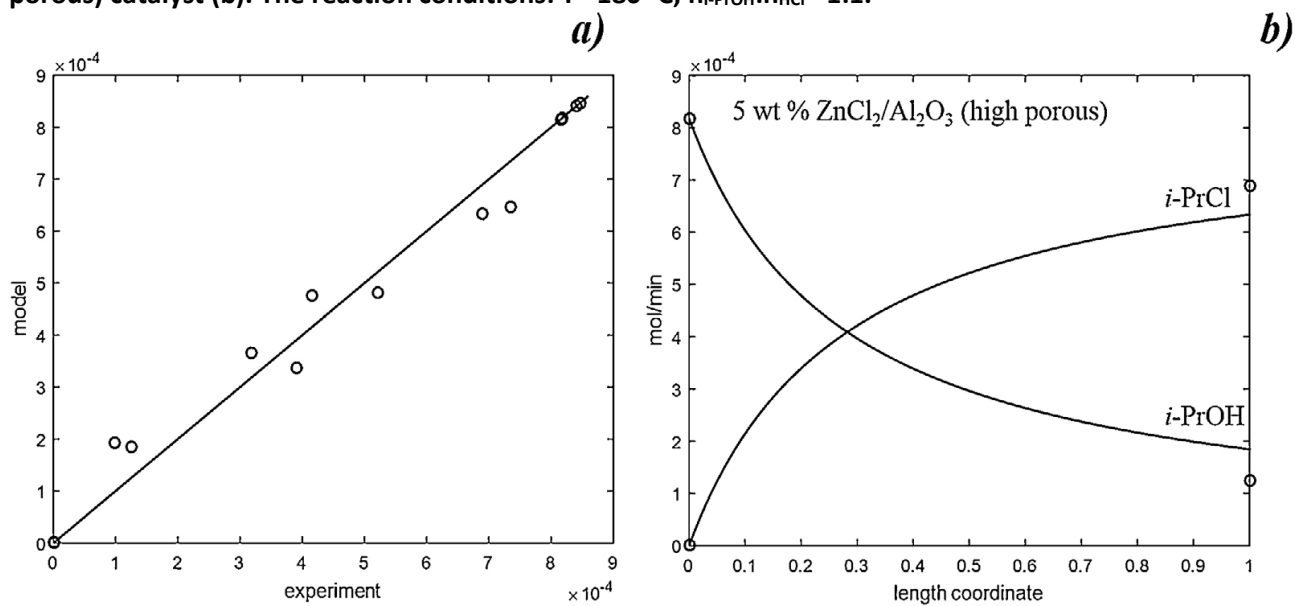


Fig. 9. Parity plot (a) and calculated molar flows inside the reactor tube over 5 wt.% ZnCl₂/Al₂O₃ (No. I) catalyst (b). The reaction conditions: T =180 °C, n_{i-PrOH}:n_{HCl} =1:1.

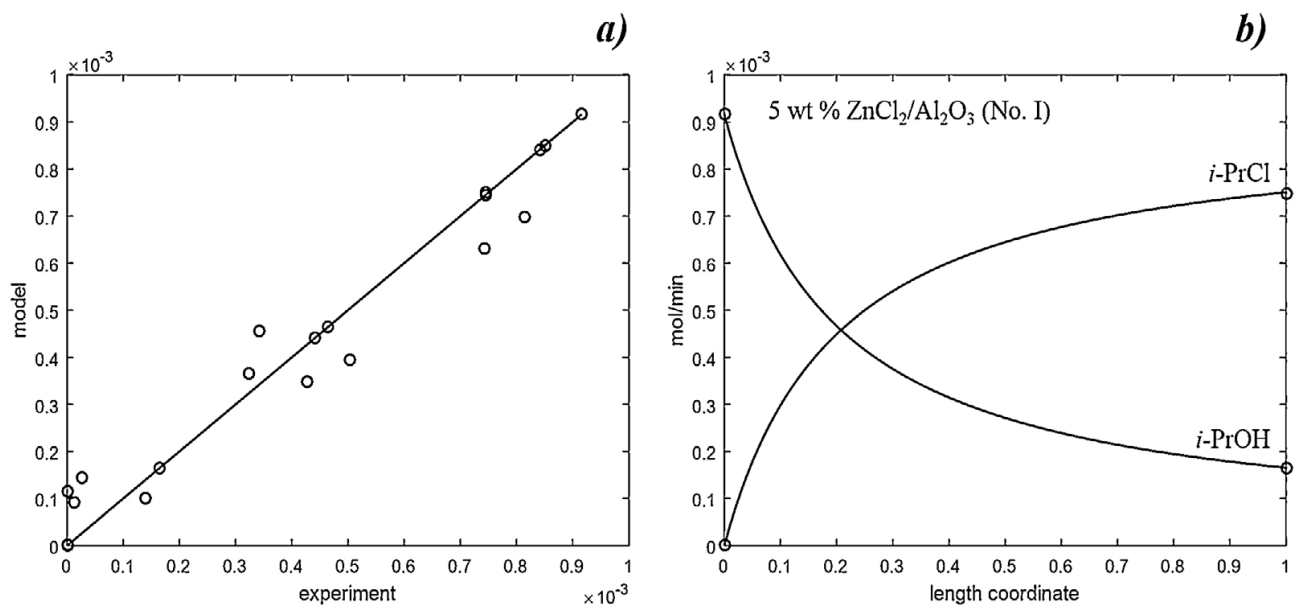


Fig. 10. Parity plot (a) and calculated molar flows inside the reactor tube over 5 wt.% ZnCl₂/Al₂O₃ (No. II) catalyst (b). The reaction conditions: T =170 °C, n_{i-PrOH}:n_{HCl} =1:1.

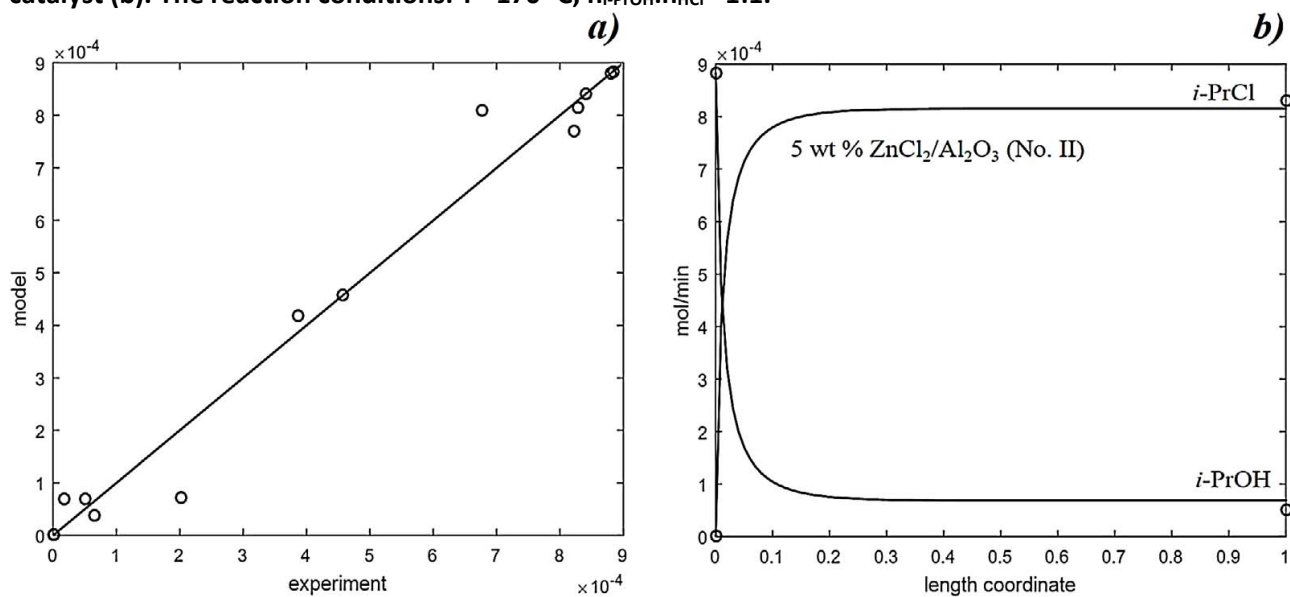


Fig. 11. Parity plot (a) and calculated molar flows inside the reactor tube over 10 wt.% ZnCl₂/C catalyst (b). The reaction conditions: T =180 °C, n_{i-PrOH}:n_{HCl} =1:1.

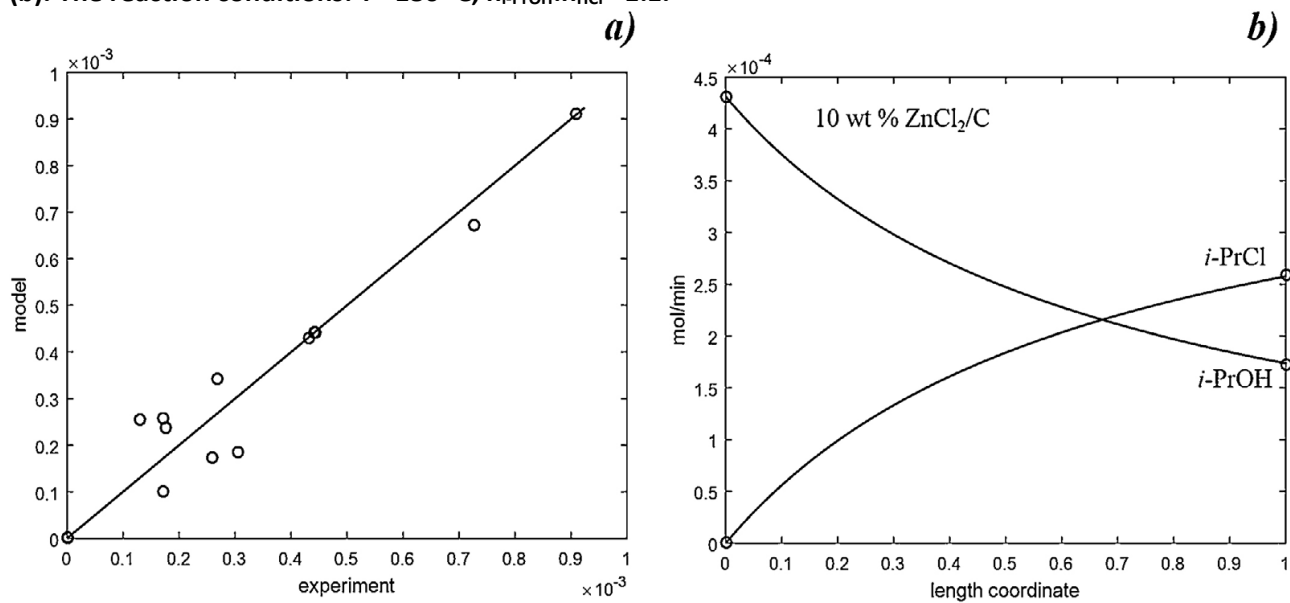


Fig. 12. Parity plot (a) and calculated molar flows inside the reactor tube over Al₂O₃ (high porous) catalyst (b). The reaction conditions: T =170 °C, n_{i-PrOH}:n_{HCl} =1:1.

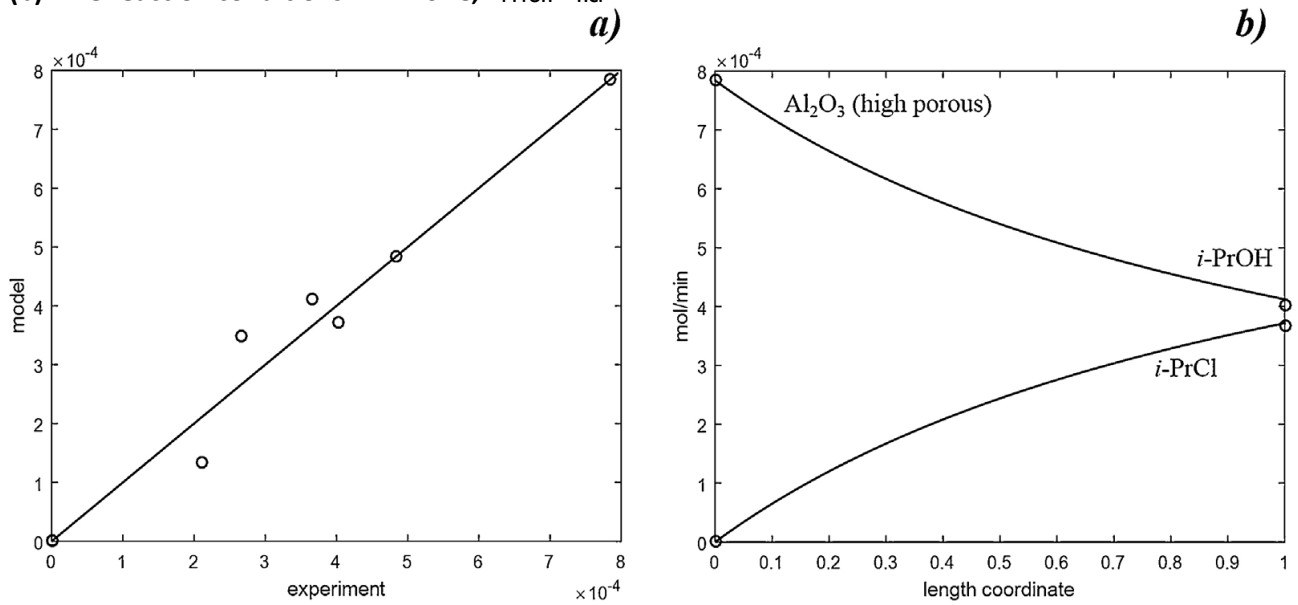


Fig. 13. Parity plot (a) and calculated molar flows inside the reactor tube over Al₂O₃ (No. I) catalyst (b). The reaction conditions: T =180 °C, n_{i-PrOH}:n_{HCl} =1:1.

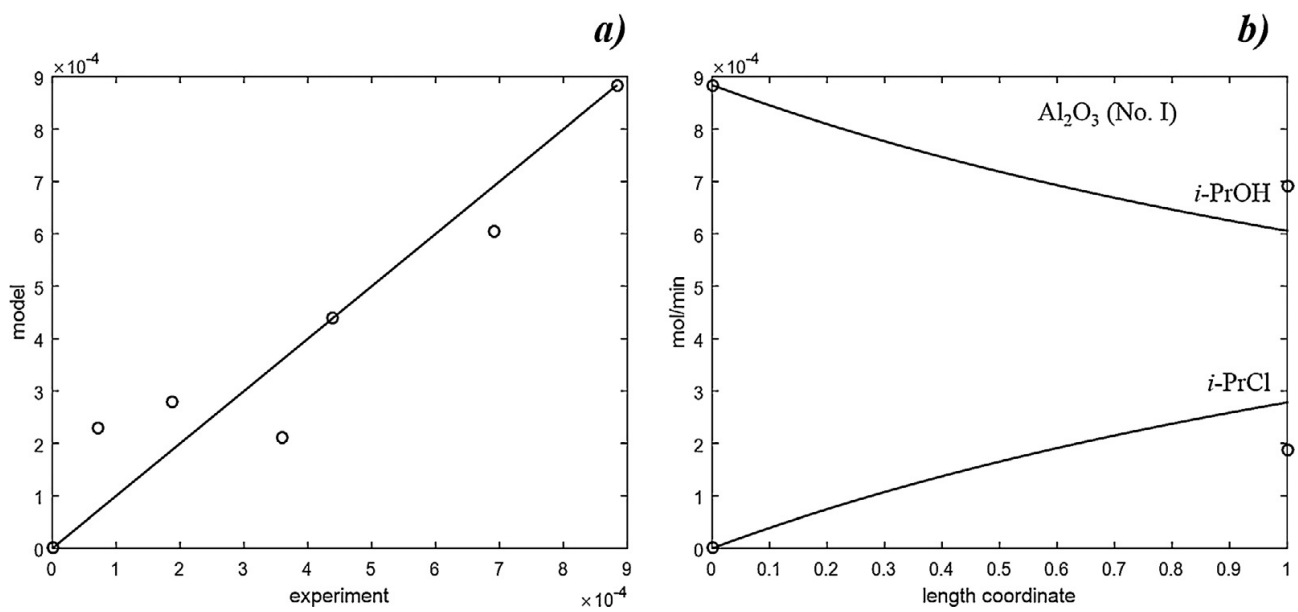


Fig. 14. Parity plot (a) and calculated molar flows inside the reactor tube over Al_2O_3 (No. II) catalyst (b). The reaction conditions: $T = 180\text{ }^\circ\text{C}$, $n_{i\text{-PrOH}}:n_{\text{HCl}} = 1:1$.

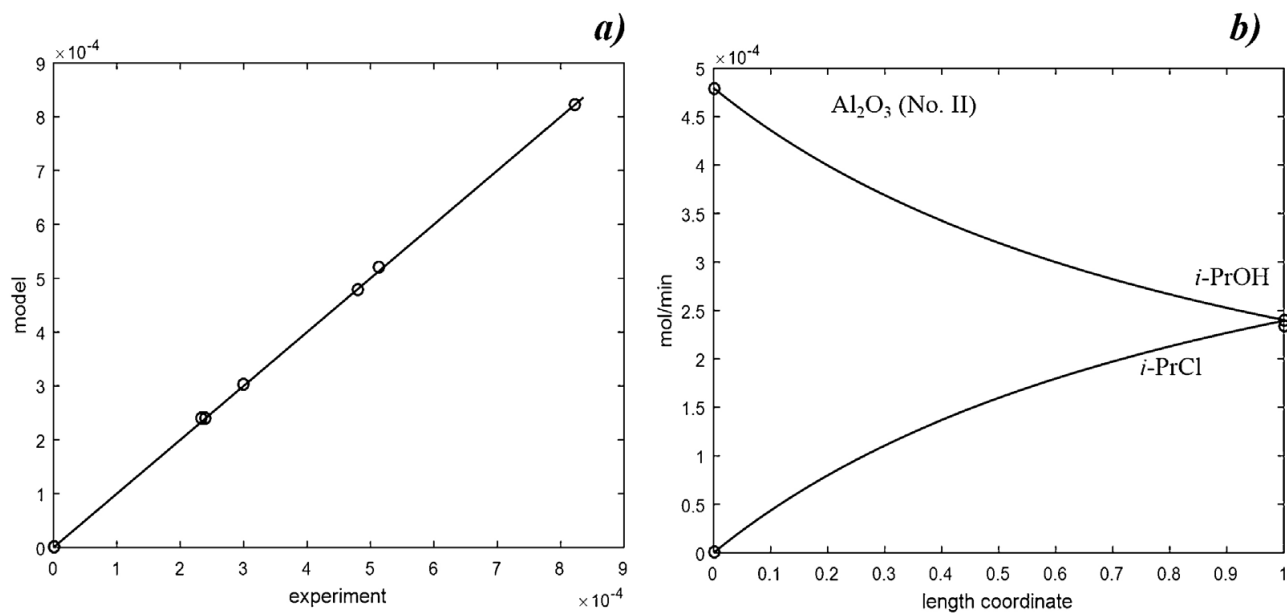
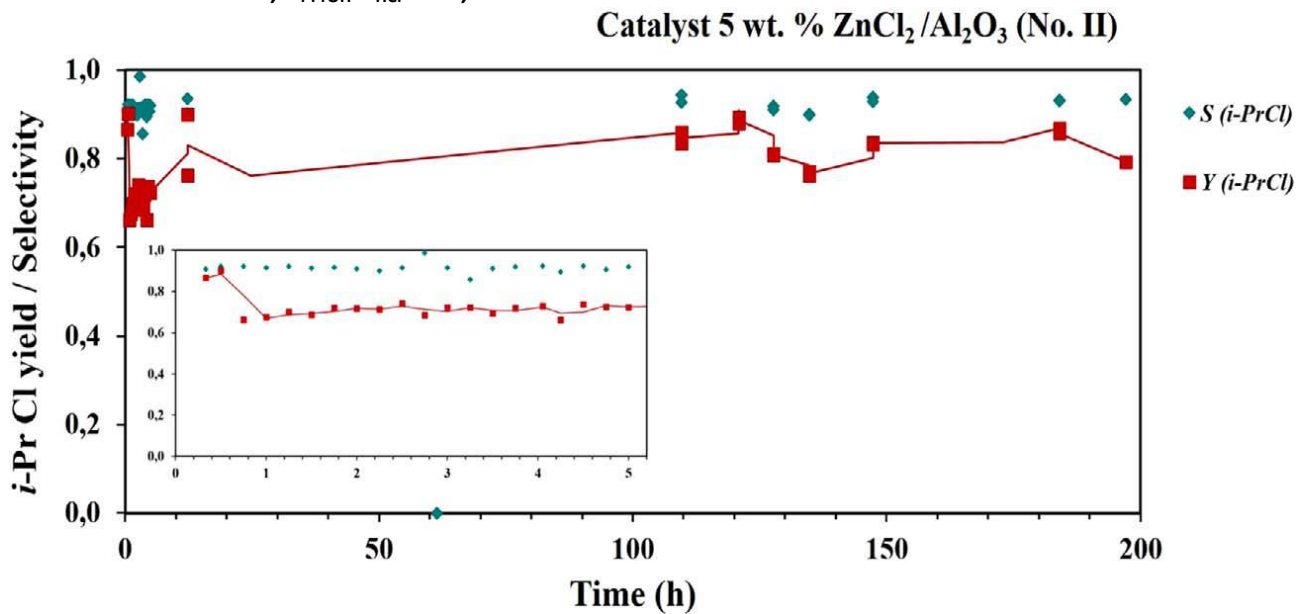


Fig. 15. Values of *i*-PrCl yield and process selectivity over 5 wt.% $\text{ZnCl}_2/\text{Al}_2\text{O}_3$ (No. II) catalyst. The reaction conditions: $T = 180\text{ }^\circ\text{C}$, $n_{i\text{-PrOH}}:n_{\text{HCl}} = 1:1$, reaction time 197 h.



Scheme 1. The proposed reaction mechanism of isopropanol hydrochlorination reaction over alumina-based catalysts in gas phase.

